Numerical modelling and fire testing of gypsum plasterboard sheathed cold-formed steel walls

Tharindu Abeysiriwardena and Mahen Mahendran

Abstract

Gypsum plasterboards are used in Light-gauged Steel Framed (LSF) walls as the primary fire-resistant material. In addition to thermal protection, they provide restraints to the cold-formed steel studs at the screw locations and improve the load-bearing capacity. In this study, three full-scale standard fire tests were conducted first to investigate the thermal and structural behaviour of LSF walls in fire. Close examination of the plasterboard joint opening up and plasterboard fall-off phenomena showed that most of the plasterboard joint compound fell-off after 17 min of fire exposure and the joint gap gradually widened afterwards. A multi-step heat transfer finite element (FE) model was developed incorporating the physical changes observed during the fire tests and validated using the test results. The important time-temperature profiles obtained from this study and past literature were compared, and idealised time-temperature profiles of wall studs were developed for use in structural FE models. Past studies involving elevated temperature structural FE models considered mainly the in-plane restraints provided by plasterboard sheathing. Hence the effects of their out-of-plane restraints were investigated using structural FE models and fire tests, and suitable out-of-plane restraint values were proposed for numerical analysis. This study has shown that out-of-plane restraints significantly reduced the lateral deflections of LSF walls and improved their fire resistance levels (FRL) when double layers of plasterboards were used. However, excessive out-of-plane restraints could adversely affect the FRL. Overall, this research has used the fire test results to enhance the understanding of the thermal and structural behaviour of LSF walls and provided useful data and recommendations for more accurate thermal and structural modelling of LSF walls.

Keywords: LSF walls; Gypsum plasterboard; Fire tests; Fire resistance; Heat transfer; Finite element analysis.

1 Introduction

The use of light gauge steel framed (LSF) wall and floor systems has become popular in the last decade due to numerous benefits they offer. These light steel frames are typically sheathed with gypsum plasterboard, which acts as the primary defence system against fire, by delaying

the temperature rise in load carrying cold-formed steel (CFS) studs. Furthermore, the use of gypsum plasterboard provides reduced construction time, ease of workmanship and thermal comfort. The core of gypsum plasterboard consists of Calcium Sulphate Dihydrate ($CaSO_4.2H_2O$), and is sandwiched between two paper layers on each side. Small amounts of glass fibre and vermiculite are added to the gypsum core to enhance its durability and fire performance. Gypsum plasterboards are available in different thicknesses and densities, and as fire-rated and non-fire rated boards. In Australia, 16 mm thick fire-rated gypsum plasterboards are commonly utilized in LSF walls to provide the required fire resistance levels (FRL).

Heat transfer occurs via three modes; conduction, convection and radiation. While conduction is the heat transfer through direct contact, convection is the transfer of heat through the motion of matter, such as gas or liquid, and radiation is the energy transfer through electromagnetic waves. Upon fire exposure, gypsum plasterboard undergoes a series of chemical reactions, releasing free and chemically bound water and as a result, its thermal and mechanical properties are changed. The use of accurate thermo-physical properties of gypsum plasterboard is essential to develop accurate and reliable heat transfer finite element (FE) models. These models can be then employed to conduct parametric studies of new LSF wall systems [1].

Many researchers have investigated the thermal properties of gypsum plasterboards [2-7], while others have further improved them using small- and full-scale experimental results [5,7]. Dodangoda et al. [7] conducted a detailed study on physical and mechanical properties of fire-rated gypsum plasterboards at ambient and elevated temperatures and proposed a suitable set of material properties for small- and full-scale heat transfer modelling.

When LSF walls are exposed to fire, plasterboard joints open up and plasterboard pieces fall-off as observed in past research studies [8-12]. This phenomenon is numerically simulated by either modifying the thermal properties of gypsum plasterboards or deleting plasterboard elements. However, due to the difficulties associated with observing the fire side plasterboard during a fire test, the propagation of joint opening-up and plasterboard piece fall-off is still not fully understood. Accurate incorporation of physical changes that occur during a fire test is essential to develop realistic heat transfer FE models of LSF walls exposed to fire on one side.

Once the time-temperature profiles are determined using experimental or numerical studies, the structural behaviour of an LSF wall can be analysed using FE analysis software such as Abaqus to determine the stud failure time (structural FRL). Mainly two methods are used to analyse the load-bearing LSF walls exposed to non-uniform temperature conditions during a

fire on one side of the wall. The first method is to explicitly model all the structural components including plasterboard sheathing interactions and non-linear screw connection behaviour. The second method is to model only the CFS stud and simulate the interaction between stud and sheathing using idealised boundary conditions. Although the first method is feasible for ambient temperature FE models, due to high nonlinearity, achieving convergence in coupled temperature-displacement FE models is challenging. Therefore, many researchers [13-18] have modelled only the CFS stud with simplified boundary conditions to investigate the structural behaviour of LSF walls exposed to non-uniform elevated temperature distributions in fire. The local and global restraints provided by plasterboard sheathing can be idealised as in-plane, out-of-plane and rotational restraints [19-21]. Although many researchers have considered the global in-plane restraints provided by plasterboard sheathing [13-18], limited studies have been conducted to investigate the effects of global out-of-plane restraints provided by plasterboard sheathing, and usually they are conservatively ignored in elevated temperature structural analyses. Dias [22] incorporated the effects of out-of-plane restraints in FE modelling and observed that the FRL was significantly increased when the spring stiffness representing the out-of-plane restraints was increased (Fig. 1). He showed that when the out-of-plane restraints were ignored, the failure times were about 40% less than the fire test results, signifying the importance of incorporating the out-of-plane restraints in the structural analysis of LSF walls exposed to non-uniform elevated temperature distributions.

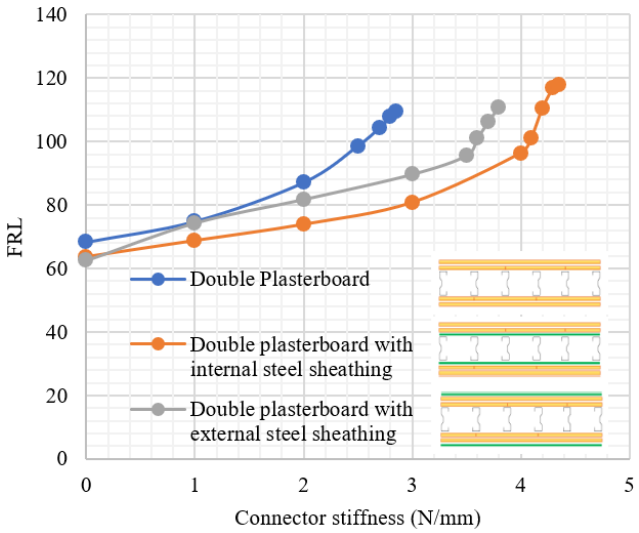

Fig. 1. Effect of out-of-plane restraint on FRL.

In this study, three full-scale fire tests were conducted under ISO 834 [23] standard fire exposure and their results are discussed first. Improvements were made to heat-transfer FE

modelling by incorporating the visual observations about the plasterboard joint opening up and plasterboard fall-off phenomena made during the full-scale fire tests. The time-temperature profiles from these tests were compared with those obtained from other full-scale standard fire tests conducted previously, based on which suitable time-temperature profiles of wall studs were proposed for structural analysis. The effects of out-of-plane restraints on the structural behaviour of CFS wall studs exposed to non-uniform elevated temperature distributions were investigated and suitable values were proposed for the structural FE modelling of single and double plasterboard sheathed LSF walls. The study presented herein provides useful information about the thermal and structural behaviour and modelling of LSF walls in fire.

2 Experimental investigation

Three full-scale standard fire tests of load-bearing LSF walls were conducted to investigate their thermal and structural behaviour in fire. The visual observations of the fire-side gypsum plasterboard layer including the plasterboard joint opening up and plasterboard fall-off phenomena, and the important time-temperature profiles for different LSF wall configurations were obtained from the fire tests. This section provides the details of test wall panels, test parameters, visual observations and time-temperature profiles from the three fire tests and a comparison with time-temperature profiles obtained by other researchers.

2.1 Test wall panels and test set-up

The LSF wall frames of dimensions 3 m x 3 m were fabricated using high strength CFS stud and track sections. Fig. 2 shows the dimensions of the CFS studs made of 0.75 mm G550 and 1.15 mm G500 web stiffened lipped channel sections. Test wall frames were made by placing six studs at 600 mm spacing and connected at the top and bottom to tracks made of 92x35x0.75 mm unlipped channel sections using screw connections. Test wall panels T1 and T2 and T3 were sheathed with single and double layers of 16 mm thick fire-rated gypsum plasterboards as shown in Fig. 3, which are the most commonly used LSF wall configurations. The first (base) and second (face) layers of gypsum plasterboards were oriented in vertical and horizontal directions, respectively, as shown in Fig. 4, and attached to the steel frame using 6g bugle head screws at 300 mm spacing. The first screw was located at 60 mm from the horizontal edge of the plasterboards when connecting the base (first) plasterboard layer to the steel frame, while it was located at 80 mm for the second plasterboard layer. Staggered screw connections were used at 200 mm spacing along the vertical plasterboard joints. The distance between the

screws and the vertical edge of the plasterboards was 10 -15 mm. Afterwards, the plasterboard joints were sealed using two coats of plasterboard joint filler and an intermediate layer of cellulose-based joint tape.

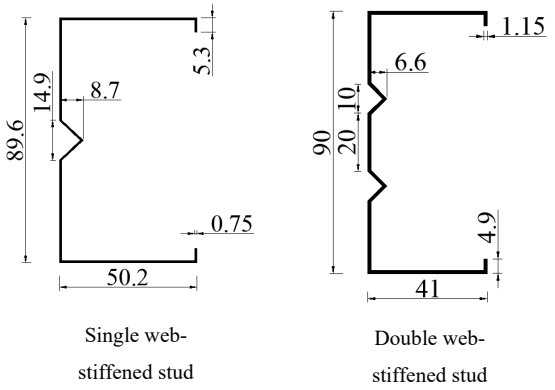

Fig. 2. External dimensions of CFS stud sections.

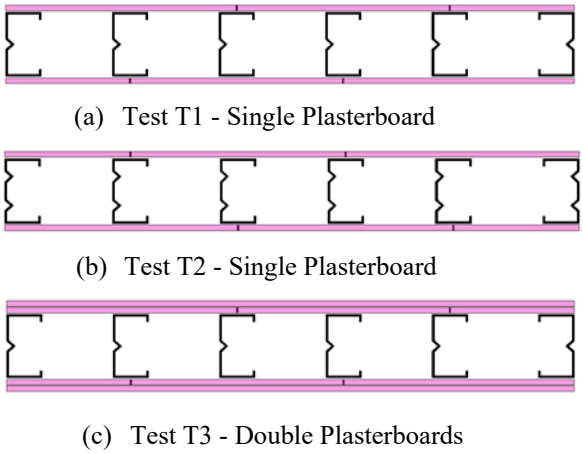

Fig. 3. Wall configurations of full-scale fire tests.

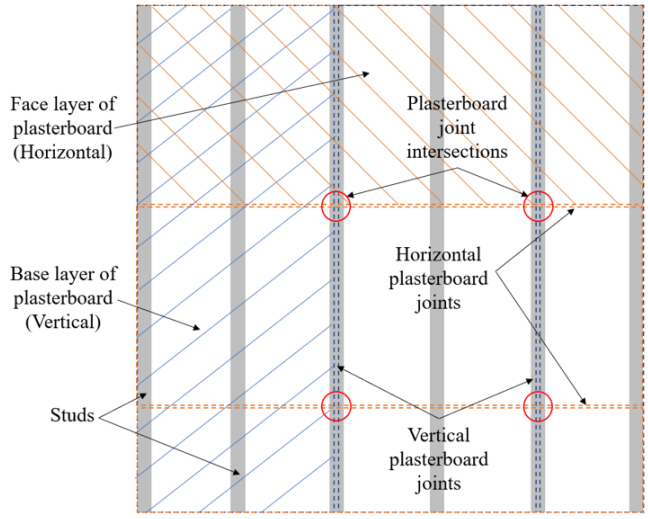

Fig. 4. Plasterboard arrangements of LSF wall made of six studs.

The 3 m x 3 m gas furnace in the QUT Wind and Fire Laboratory was used to test the LSF walls under ISO 834 [23] standard fire curve (Fig. 5). The top of the LSF wall was secured against the rigid steel girder located at the top and a pre-determined axial compression load based on a load ratio of 0.4 (40% of the ambient temperature compression capacity) was applied to each stud using the single acting hydraulic rams at the bottom. This load was maintained during the fire test until the failure of one or more studs occurred. The walls were subjected to two pre-loading cycles of 2% of their ambient compression capacity, prior to the fire test, to mitigate the effect of any slackness or lose connections.

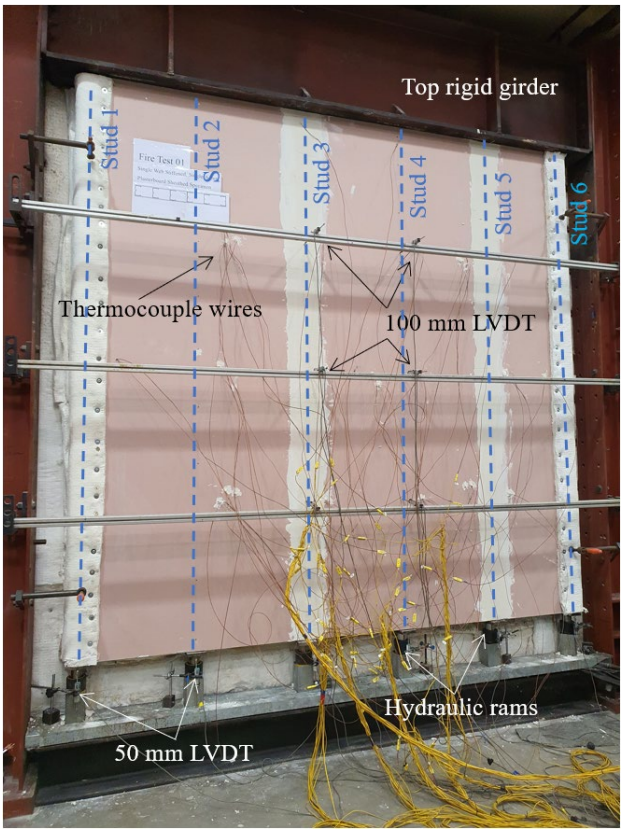

Fig. 5. Full-scale fire test arrangement.

Axial displacements of all the studs and lateral mid-height displacements of the wall were measured using 50 mm and 100 mm LVDTs, respectively, as shown in Fig. 5. To measure the temperature profiles throughout the wall panel, K-type thermocouples were attached on the surfaces of gypsum plasterboards and, web and flange elements of the studs, as illustrated in Fig. 6. In addition, for the double plasterboard sheathed wall, extra thermocouples were attached to the studs along the plasterboard joint intersections, as shown in Fig. 4. Fig. 7 illustrates how thermocouples were connected to gypsum plasterboards and CFS studs. A camera with a telephoto lens was attached to one of the observation ports of the furnace to

monitor the behaviour of the fire side plasterboard layers during the fire tests. The camera equipment was constantly cooled using cold air to prevent any damage from convective and radiation heat.

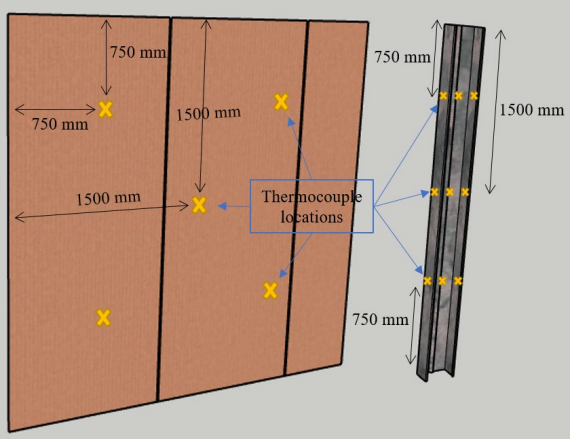

Fig. 6. Thermocouple locations.

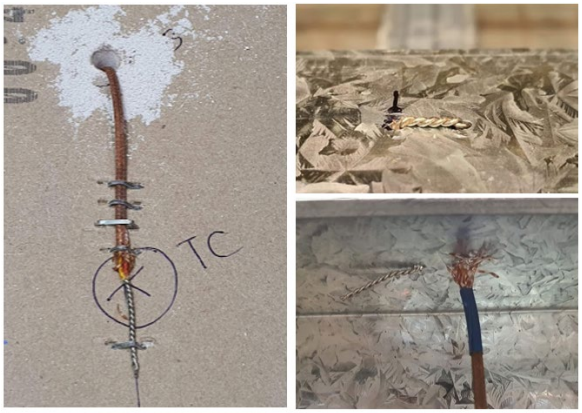

(a) (b)

Fig. 7. Thermocouples connected to a) plasterboards and b) studs.

2.2 Test results

In all three fire tests, the web stiffened studs located along the fire side vertical plasterboard joints failed by distortional buckling (Fig. 8), and their failures occurred after 43 min (Stud 4 at one third length from the top), 34 min (Stud 3 at 600 mm from the top) and 107 min (Stud 4 at one third length from the bottom), respectively. Distortional buckling halfwave lengths of single and double web-stiffened studs were approximately 300 and 150 mm, respectively. There were no insulation or integrity failures. Failure times of Fire Tests T1 and T2 were similar (34 and 43 min) indicating the minimal influence of the type of stud section, while the significant increase in the failure time of Fire Test T3 (43 to 107 min) indicates the benefit of

having two plasterboard sheathing. In all the tests, the test wall deformed away from the furnace and failed, i.e. in the opposite direction of thermal bowing.

Fig. 8. Distortional buckling failures of tested LSF walls.

2.3 Visual observations of fire side plasterboard surface

The behaviour of the fire side plasterboard surface was captured well during Fire Tests T2 and 3. Fig. 9 illustrates the visual observations of Fire Test T2 (single plasterboard sheathed wall) until failure. The paper layer of the fire side plasterboard started burning after 3 min from the start of the test, as the furnace temperature rose beyond 250 ℃, and in about 30 s the paper layer was completely burnt. The edges of the vertical plasterboard joint compound started to detach from the plasterboard surface at 10th min, due to the different thermal expansion rates of gypsum plasterboard and joint filler compound. Next, micro-crack formation was observed throughout the plasterboard joint filler at about 15th min and small plasterboard joint pieces started falling at random locations. Detachment and fall-off of big pieces of vertical plasterboard joint filler occurred by about 17th min, except for some pieces along the edges, thus exposing most of the plasterboard gap in the middle. Finally, by 23rd min, plasterboard joint filler at the edges also fell-off, completely exposing the studs at the vertical plasterboard joints to direct flames through the gap. Due to this flame intrusion, the temperatures of the hot flanges of these studs increased rapidly compared to the adjacent studs, which led to differential thermal bowing. Due to the evaporation of free and chemically bound moisture, gypsum plasterboards are subjected to shrinkage at elevated temperatures [7]. As a consequence of differential thermal bowing and plasterboard shrinkage, a gradual increase in plasterboard joint gap size was observed, allowing further heat penetration through it. At 34 min, the hot flange of Stud 3, which was located along the middle plasterboard joint, failed and deformed away from the furnace and at the same time, the detached plasterboard cracked and moved towards the furnace.

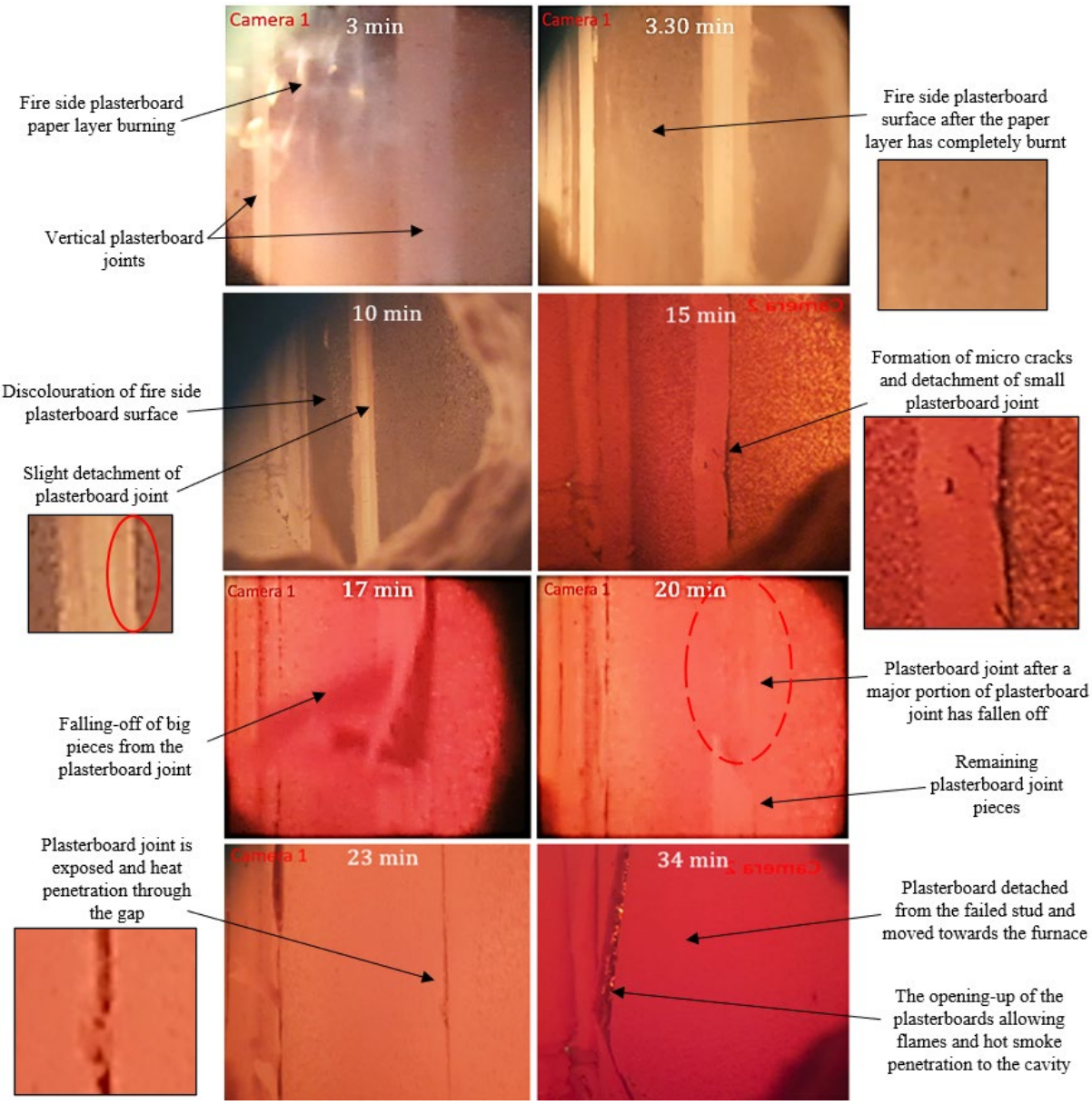

Fig. 9. Observations of fire side plasterboard of single plasterboard sheathed wall panel in Fire Test T2.

The visual observations of Fire Test T3 (double plasterboard sheathed wall) are illustrated in Fig. 10. Similar to the observations of single plasterboard sheathed wall, the fire side paper layer started burning at about 2 min and 20 s and finished within a minute. At 7th min, small cracks appeared in the horizontal plasterboard joint filler and at 11th min small pieces of it started falling off. Severe plasterboard joint fall-off was observed around 13th min and by 17th min, the joint compound was almost completely detached. Similar to the observation of Fire Test T2, a gradual increase in plasterboard gap size was observed with time due to the thermal bowing of studs and shrinkage of plasterboards. One of the middle two studs failed at 107 min and due to its sudden movement at failure, a sizeable portion of fire side gypsum plasterboard

fell-off exposing the cavity. It is important to note that, plasterboard fall-off was not observed at random locations away from the plasterboard joints, and the most vulnerable location of studs in a typical LSF wall exposed to fire is its plasterboard joints.

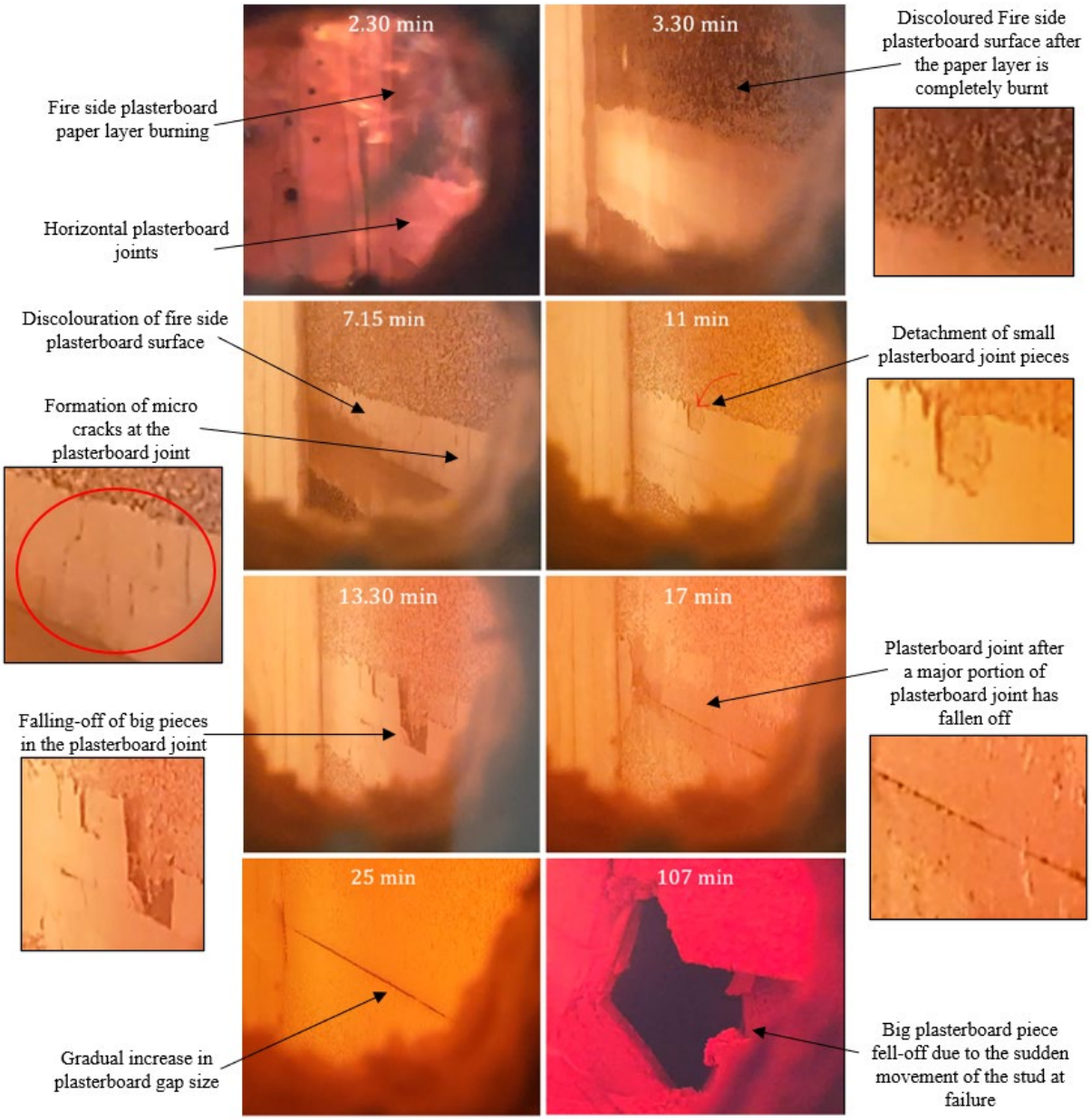

Fig. 10. Observations of fire side plasterboard of double plasterboard sheathed wall panel in Fire Test T3.

2.4 Mechanisms of heat transfer through an LSF wall

Fig. 11 illustrates the mechanisms of heat transfer from the fire side to the ambient side through an LSF wall cross-section with and without plasterboard joint opening. The heat is initially transferred from the furnace to the fire side plasterboard through convection and radiation and

then it is propagated to the fire side cavity surface of the plasterboard through conduction. Next, the fire side cavity plasterboard surface transmits the heat to the ambient side cavity plasterboard surface and the hot flange of the stud through radiation and conductance, respectively. Convective heat transfer through the cavity is considered to be negligible since the air flow inside the cavity is insignificant [1]. The stud conducts the heat from the hot flange to the cold flange and then to the ambient cavity side of the plasterboard through conductance. Subsequently, the ambient side plasterboard conducts the heat from its cavity surface to the ambient surface through conductance and finally, the heat is released from the ambient side plasterboard surface through radiation and convection. As discussed in Section 2.3, most of the plasterboard joint fell-off after about 17 min of ISO 834 [23] standard fire exposure, and thus directly exposing the stud hot flange to the flames. Hence, after the joint fall-off, the middle portion of the stud's hot flange starts absorbing the heat directly from convection and radiation.

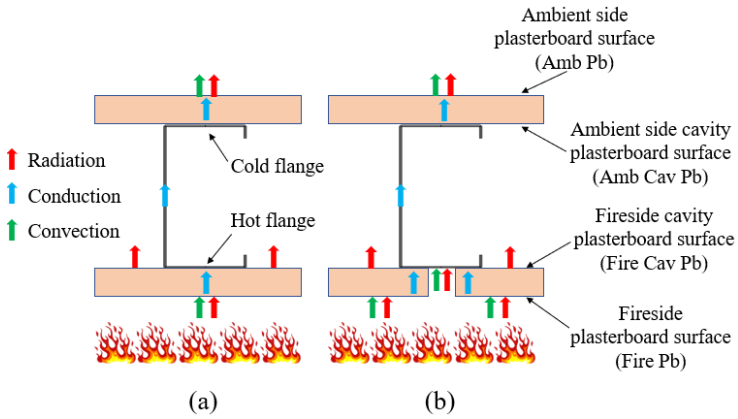

Fig. 11. Heat transfer through LSF wall panel a) without and b) with plasterboard joint opening

2.5 Comparison of time-temperature profiles

In recent years, many fire tests have been conducted to investigate the behaviour of LSF walls in fire [24-32]. In this section, the time-temperature profiles from the fire tests conducted in this study and previous studies are compared to gain a better understanding of heat transfer through LSF walls. Details of the fire tests selected from previous studies are summarised in Table 1, where RHS, SHS and LCS indicate rectangular hollow, square hollow and lipped channel sections (no stiffeners), respectively. All the tested LSF walls in Table 1 were cavity insulated.

Table 1: Details of fire tests selected for comparison.

Previous study	Test number	Section Type	h (mm)	b (mm)	a (mm)	t (mm)	Steel Grade	No of Pb. layers	LSF wall panel sizes (m)
Ariyanayagam and Mahendran [28]	3	LCS	92	35	8	0.55	G300	Single	3 x 3
	5	LCS	92	35	8	0.55	G300	Double	3 x 3
Ariyanayagam and Mahendran [17]	1	LCS	92	35	8	0.55	G300	Single	3 x 3
	3	LCS	92	35	8	1.15	G300	Single	3 x 3
Tao et al. [32]	2	SHS	90	90	-	2	G450	Double	3 x 3
	4	RHS	150	50	-	2	G450	Double	3 x 3
Gunalan et al. [26]	2	LCS	90	40	15	1.15	G500	Single	2.4 x 2.4
	3	LCS	90	40	15	1.15	G500	Double	2.4 x 2.4

Note: h = web height, b = flange width, a = lip height in LCS and t = thickness.

Fig. 12 compares the key plasterboard surface time-temperature profiles of 3 m x 3 m single plasterboard sheathed LSF walls from Fire Tests T1 and T2 in this study, Test 3 in Ref. [28] and Tests 1 and 3 in Ref. [17]. Similarly, Fig. 13 compares these time-temperature profiles of 3 m x 3 m double plasterboard sheathed LSF walls from Fire Test T3, Test 5 in Ref. [28] and Tests 2 and 4 in Ref. [32]). In Figs. 12 and 13, the abbreviations used to represent the different plasterboard surfaces are shown in Fig. 11. All the test walls were exposed to the standard fire curve on one side using the 3 m x 3 m furnace in the QUT Wind and Fire Laboratory. Interestingly, Figs. 12 and 13 show that the plasterboard surface time-temperature profiles obtained by different researchers were almost identical for a given plasterboard configuration, which signifies the high repeatability of the tests and consistency of gypsum plasterboard material properties. As observed in Section 2.3, the fire side plasterboards are often detached from the failed stud at its failure, due to the sudden deformations, allowing flames and hot gasses to enter the cavity. As a result, in some tests, sudden temperature rises are observed in the cavity near the failure time. Even though the geometry and thicknesses of studs used in these tests are different (Table 1), the plasterboard surface temperatures are almost identical, which indicates the heat transfer in the cavity through convection and radiation governs the temperature profiles of the plasterboard surfaces rather than conduction through stud sections.

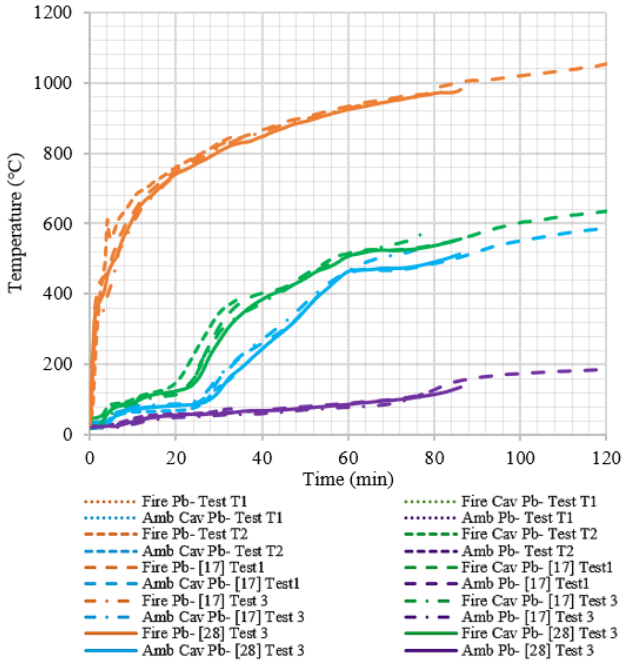

Fig. 12. Time-temperature profiles of 3m x 3 m single plasterboard sheathed walls.

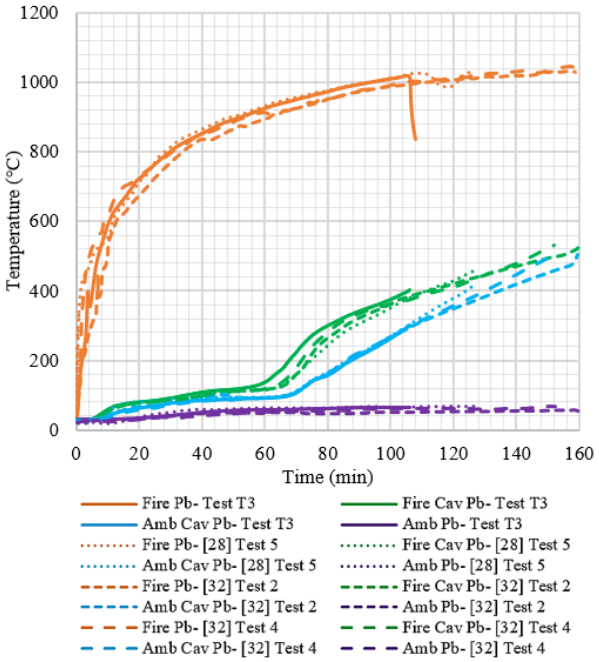

Fig. 13. Time-temperature profiles of 3 m x 3 m double plasterboard sheathed walls.

Gunalan et al. [26] conducted similar fire tests of 2.4 m x 2.4 m LSF walls using a 2.4 m x 2.4 m gas furnace about 10 years ago. Their time-temperature profiles are compared with those of 3 m x 3 m LSF wall tests conducted by others [17, 28, 32] (Table 1) in Fig. 14, which exhibits a significant difference. The reason for this difference could be smaller cavity size, changes in plasterboard material properties or other problems associated with furnace and instrumentation. For single plasterboard sheathed walls, the difference in cavity temperature is significantly lower in Gunalan et al.'s [26] test results, and therefore using them in coupled temp-displacement analysis could result in lower thermal bowing and unsafe failure time predictions.

In contrast, for double plasterboard sheathed walls, significantly high cavity temperatures were obtained in Gunalan et al. [26], which could lead to overconservative predictions of failure times and uneconomical designs. Therefore, it is important to use the time-temperature profiles of the recent fire tests of 3 m x 3m walls for numerical model validation and parametric studies.

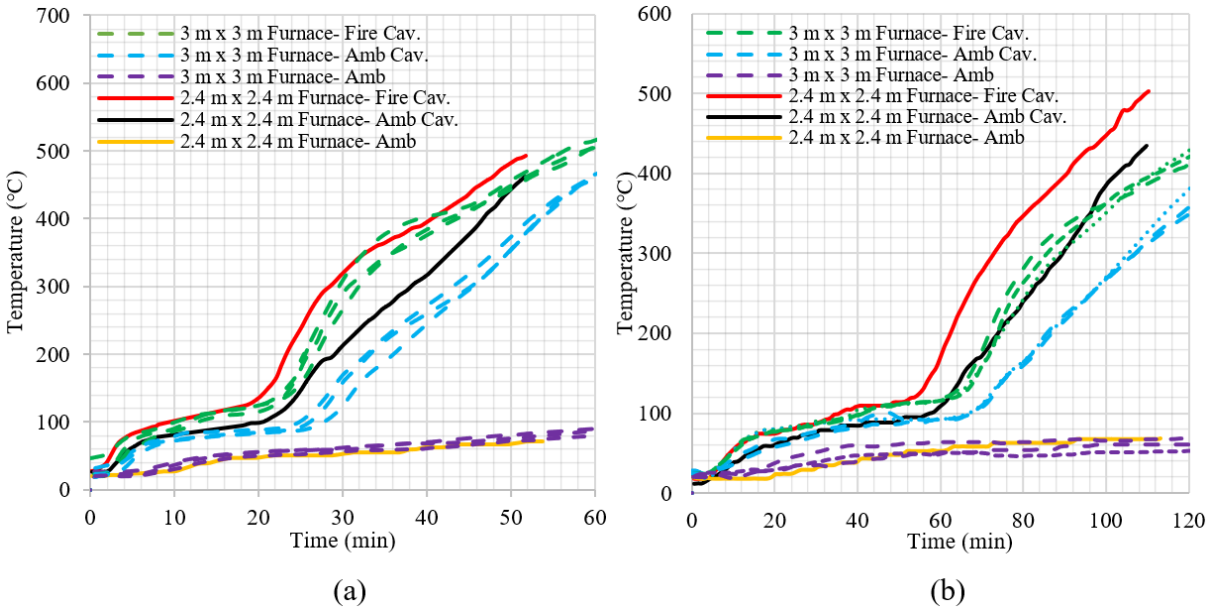

Fig. 14. Comparison of time-temperature profiles from 2.4 m x 2.4 m and 3 m x 3 m furnace tests a) single plasterboard sheathed b) double plasterboard sheathed walls.

Effects of stud thickness were also investigated using time-temperature profiles. Fig. 15 compares the hot and cold flange time-temperature profiles of the studs, not located at the plasterboard joints, in single plasterboard sheathed walls obtained in this study (0.75 and 1.15 mm studs in Fire Tests 1 and 2) and Ariyanayagam and Mahendran [17] (0.55 and 1.15 mm studs of Tests 1 and 3). The difference between hot and cold flange temperatures was almost similar for all the stud thicknesses. Hence, the effect of stud thickness on time-temperature profiles can be considered to be negligible for LSF walls made of open lipped channel studs.

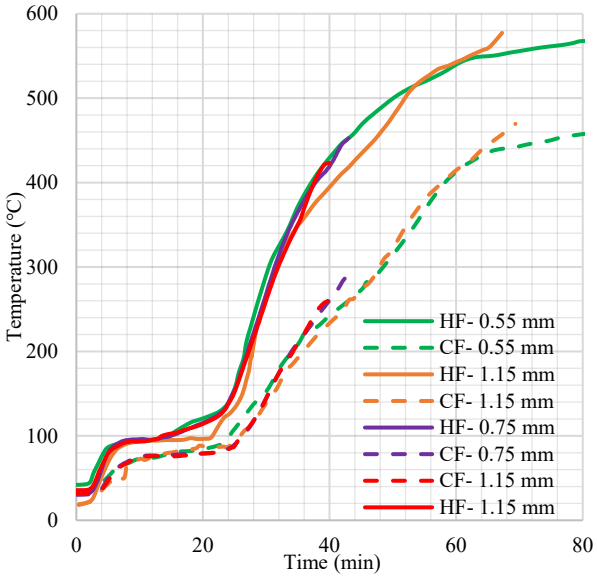

Fig. 15. Effects of stud thickness on the time-temperature profiles of hot and cold flanges.

In LSF walls, the heat is transferred from the fire side cavity plasterboard surface to the hot flange of the studs. If the fire side plasterboard is undamaged, the hot flange temperature should be less than or equal to the fire side cavity plasterboard surface temperature. However, comparison of the hot flange and the fire side plasterboard cavity temperatures for single plasterboard sheathed walls (Fire Tests T1 and T2 and those in Table 1) show that after 17 min, a substantial temperature difference is observed between them, due to the opening of vertical plasterboard joints. Therefore, when numerically simulating the heat transfer through single plasterboard sheathed walls, the joint opening behaviour must be incorporated to obtain accurate results. Ariyanayagam et al. [9] also observed that the most vulnerable place in a typical LSF wall is the plasterboard joint and proposed innovative wall configurations to overcome the associated detrimental effects.

For double plasterboard sheathed LSF walls, the temperatures of the hot flange and the fire side plasterboard cavity were similar, as shown in Fig. 16 based on the results from Fire Test T3 and other tests in Table 1. This is because the studs are well protected by the base layer of the plasterboards, as shown in Fig. 4, even after the horizontal plasterboard joint of the face layer has completely fallen-off. However, as illustrated in Fig. 17, a highly localised, but substantial temperature increment was observed at the intersections of the vertical (base layer) and horizontal (face layer) plasterboard joints (Fig. 4).

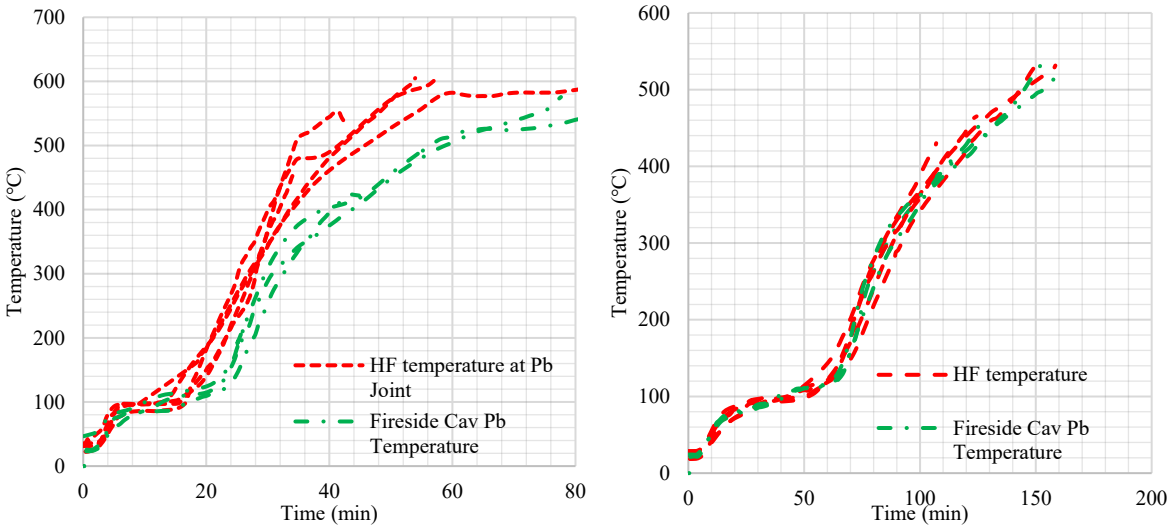

(a) (b)

Fig. 16. Comparison of time-temperature profiles of fire side cavity plasterboard surface and hot flange in a) single and b) double plasterboard sheathed walls.

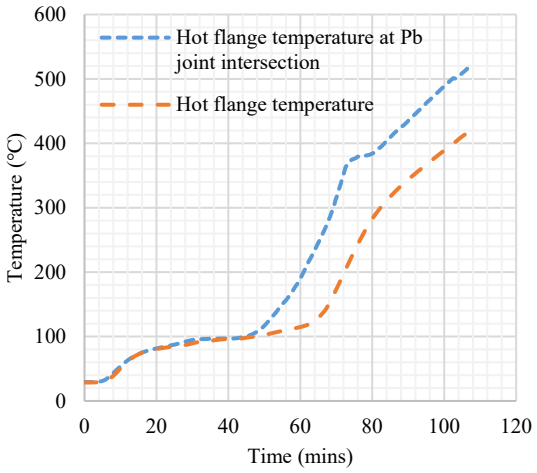

Fig. 17. Hot flange time-temperature profiles at the plasterboard joint intersection of double plasterboard sheathed wall.

2.6 Idealised time-temperature profiles

Accurate time-temperature profiles are essential for predicting the failure times of LSF walls. Using the full-scale fire test results, idealised time-temperature profiles were developed for hot and cold flanges using the upper bound temperature envelope as given in Eqs. (1-23). Fig. 18. shows an example of how the upper bound temperature envelope was derived for the hot flange of the single plasterboard sheathed studs located at and away from the plasterboard joint. These time-temperature profiles are valid for 0.5 to 1.15 mm thick lipped channel studs sheathed with

16 mm thick gypsum plasterboards (density of 13 kg/m^2) under standard fire exposure. Further specifications of gypsum plasterboards used in this study are given in Section 3.1.

LSF walls sheathed with single plasterboard on both sides,

Hot flange temperature of studs at plasterboard joint,

$$T_{HF} = 20.48\,t - 207.1 \quad \text{for} \quad 15 \le t < 36 \quad (1)$$

$$T_{HF} = 3.64\,t + 399.1 \quad \text{for} \quad 36 \le t < 80 \quad (2)$$

Cold flange temperature

$$T_{CF} = 2.22\,t + 46.7 \quad \text{for} \quad 15 \le t < 24 \quad (3)$$

$$T_{CF} = 12.73\,t - 205.5 \quad \text{for} \quad 24 \le t < 35 \quad (4)$$

$$T_{CF} = 8.33\,t - 51.7 \quad \text{for} \quad 35 \le t < 62 \quad (5)$$

$$T_{CF} = 2.5\,t + 310 \quad \text{for} \quad 62 \le t < 80 \quad (6)$$

Hot flange temperature of intermediate studs with no plasterboard joints.

$$T_{HF} = 5\,t + 25 \quad \text{for} \quad 15 \le t < 23 \quad (7)$$

$$T_{HF} = 19.17\,t - 300.8 \quad \text{for} \quad 23 \le t < 35 \quad (8)$$

$$T_{HF} = 10\,t + 20 \quad \text{for} \quad 35 \le t < 50 \quad (9)$$

$$T_{HF} = 3.33\,t + 353.3 \quad \text{for} \quad 50 \le t < 80 \quad (10)$$

Cold flange temperature

$$T_{CF} = 0.83\,t + 67.5 \quad \text{for} \quad 15 \le t < 27 \quad (11)$$

$$T_{CF} = 11.54\,t - 221.5 \quad \text{for} \quad 27 \le t < 40 \quad (12)$$

$$T_{CF} = 9.55\,t - 141.8 \quad \text{for} \quad 40 \le t < 62 \quad (13)$$

$$T_{CF} = 2.61\,t + 288.1 \quad \text{for} \quad 62 \le t < 80 \quad (14)$$

LSF walls sheathed with double plasterboards on both sides,

$$T_{HF} = 0.98\,t + 65.4 \quad \text{for} \quad 15 \le t < 56 \quad (15)$$

$$T_{HF} = 6.33\,t - 234.3 \quad \text{for} \quad 56 \le t < 105 \quad (16)$$

$$T_{HF} = 2.6\,t + 157 \quad \text{for} \quad 105 \le t < 150 \quad (17)$$

Hot flange temperature of studs at plasterboard joint intersection,

$$T_{HF} = 1.14\,t + 62.9 \quad \text{for} \quad 15 \le t < 50 \quad (18)$$

$$T_{HF} = 10.4\,t - 400 \quad \text{for} \quad 50 \le t < 75 \quad (19)$$

$$T_{HF} = 4.89\,t + 13.3 \quad \text{for} \quad 75 \le t < 150 \quad (20)$$

Cold flange temperature

$$T_{CF} = 0.76\,t + 55.6 \quad \text{for} \quad 15 \le t < 65 \tag{21}$$

$$T_{CF} = 5.2\,t - 233 \quad \text{for} \quad 65 \le t < 90 \tag{22}$$

$$T_{CF} = 4\,t - 125 \quad \text{for} \quad 90 \le t < 150 \tag{23}$$

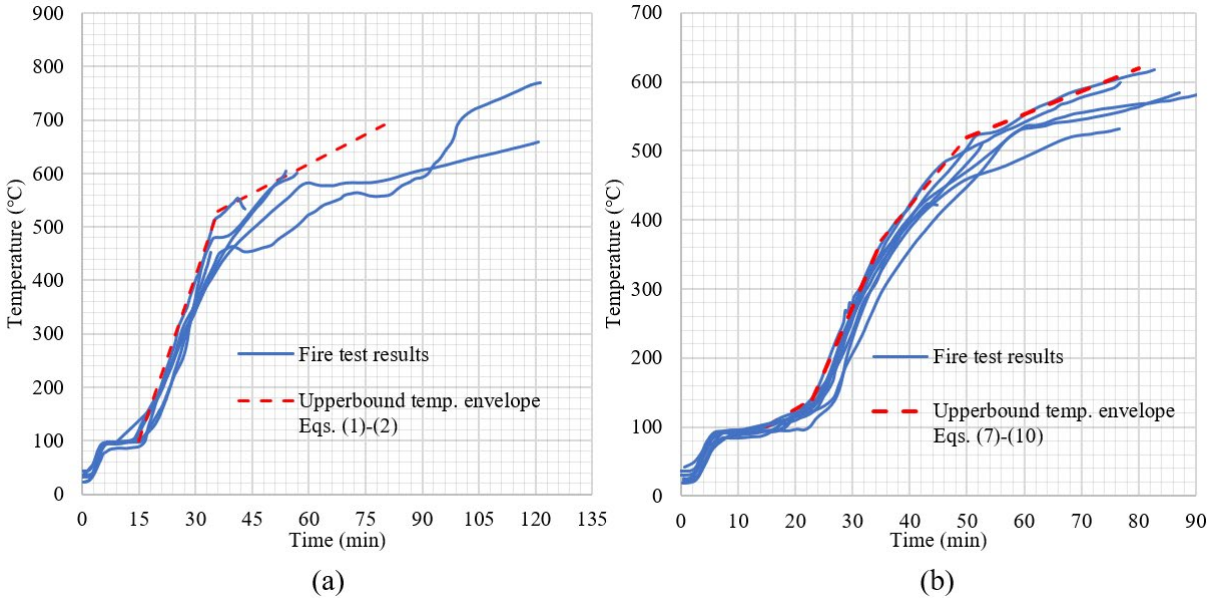

Fig. 18. Hot flange time-temperature profiles for single plasterboard sheathed studs a) at the plasterboard joint and b) away from the plasterboard joint.

3 Heat transfer modelling of LSF walls

Rusthi et al. [1] proposed a method to accurately simulate heat transfer across an LSF wall using Abaqus 3-D FE software. In this section, the details of the heat transfer model developed, updated material properties of LSF wall components and improvements made to heat transfer modelling techniques incorporating the visual observations in the fire tests are presented.

3.1 Material properties

The use of appropriate elevated temperature material properties is essential to produce accurate numerical outputs. Eqs. (24-26) show how the rates of conduction, convection and radiation heat transfer are calculated using thermal conductivity (k), temperature gradient (dT/dx), film coefficient (h), surface emissivity (ε) and the Stephan Boltzmann constant (σ). Heat transfer analysis results are more sensitive to thermal conductivity and specific heat values rather than relative emissivity, convective coefficient and density values [7].

$$q_{conduction} = -k(dT/dx) \tag{24}$$

$$q_{convection} = h(T_{hot} - T_{cold}) \tag{25}$$

$$q_{radiation} = \varepsilon\sigma\left({T_{hot}}^4 - {T_{cold}}^4\right) \tag{26}$$

Specific heat (C_p) and thermal conductivity (k) values of steel were obtained from Eurocode 3 Part 1-2 [33] as shown in Eqs. (27-30) and Eqs. (31-32), respectively. A constant density value of 7850 kg/m^3 was used for steel in the FE model throughout the analysis.

$$C_p = 425 + 7.73 \times 10^{-1}T - 1.69 \times 10^{-3}T^2 + 2.22 \times 10^{-6}T^3 \quad 20℃ \leq T < 600℃ \quad (27)$$

$$C_p = 666 + 13002/(738 - T) \quad 600℃ \leq T < 735℃ \quad (28)$$

$$C_p = 545 + 17820/(T - 731) \quad 735℃ \leq T < 900℃ \quad (29)$$

$$C_p = 650 \quad 900℃ \leq T < 1200℃ \quad (30)$$

$$k = 54 - 3.33 \times 10^{-2}T \quad 20℃ \leq T < 800℃ \quad (31)$$

$$k = 27.3 \quad 800℃ \leq T < 1200℃ \quad (32)$$

Dodangoda et al. [7] investigated the physical and mechanical properties of gypsum plasterboards at ambient and elevated temperatures and proposed a suitable set of material properties for small- and full-scale heat transfer analyses. They proposed idealised gypsum plasterboard density values at elevated temperatures (Table 2) for elevated temperature numerical models of full-scale tests. Specific heat values of gypsum plasterboards were measured using differential scanning calorimeter at temperatures up to 1200 ℃ in accordance with ASTM E1269 [34] and the proposed idealised values are given in Table 3. The thermal conductivity of the gypsum plasterboard was derived only up to 500 ℃ using the measured thermal diffusivity values. A core sample of 100 mm square and 2 mm thickness is analysed using laser flash analysis (LFA) to measure the thermal diffusivity variation with temperature. However, this small core sample does not accurately represent the behaviour of a complete gypsum plasterboard and the thermal conductivity values above 500 ℃ are necessary for numerical modelling. Therefore, idealised thermal conductivity variation is often derived using the results from experimental heat transfer studies because the net effect of moisture migration, ablation, crystalline structure, radiation in the voids and formation of micro-cracks can be taken into account using this method. As described in Section 2.5, a sudden increase in temperatures can be observed in the fire tests just before the failure of the studs due to joint opening or plasterboard fall-off. Many researchers [2-3, 5, 7, 17, 35] have simulated this behaviour by providing a sharp increase in thermal conductivity values near the end of the simulation. Therefore, the use of those proposed thermal conductivity values is suitable only when the failure time of the current analysis is lower than the experimental result used for the thermal conductivity calibration.

Table 2. Recommended idealised density values for full-scale numerical models [7]

Temperature °C	Density (kg/m^3)
23	812.5
120	810
155	725
177	687
213	683
655	676
752	663
885	658
935	648
1200	638

Table 3. Recommended specific heat values for full-scale numerical models [7]

Temperature °C	Specific heat J/(kg·K)
23	1000
80	1270
100	1510
113	2280
152	13500
165	10000
173	10800
195	2000
215	1210
250	1000
1200	1000

Using the results of recently conducted full-scale fire tests of 3 m x 3 m LSF walls and more than 50 FE analyses, suitable thermal conductivity values were proposed for single and double-layered plasterboard sheathed walls (Table 4) to achieve a good agreement between test and FE analysis results. The proposed apparent thermal conductivity values for double plasterboard configurations are higher than those proposed for single plasterboard configurations beyond 800 ℃. When considering the fire side plasterboard in single plasterboard sheathed LSF walls, the heat from the furnace is transferred through its cross-section to the cavity. However, in

double plasterboard sheathed LSF walls, the heat transferred to the fire side face layer plasterboard is transferred first to the base plasterboard layer and then to the cavity. Hence, the face layer of fire side gypsum plasterboard is subject to a more severe elevated temperature distribution. Furthermore, Batista (2015) showed that when fire exposure times are high, the strength and stiffness of gypsum plasterboards are reduced even at constant temperatures. Since the rate of heat transfer through double plasterboards is less than that of single plasterboards, when single and double plasterboard sheathed walls reach a similar hot flange temperature, higher damage is expected on the fire side plasterboards of double plasterboard sheathed wall. Therefore, the proposed apparent thermal conductivity values of double plasterboard sheathed walls are higher than those of single plasterboard sheathed walls.

Table 4. Proposed thermal conductivity values for single and double plasterboard sheathed walls.

Temperature °C	Thermal conductivity (W/m.K)	
	Single Plasterboard	Double Plasterboards
23	0.26	0.26
80	0.26	0.26
150	0.12	0.12
215	0.12	0.12
400	0.15	0.15
700	0.20	0.15
800	0.180	0.15
880	0.164	0.30
900	0.16	0.313
1200	0.16	0.50

Fig. 20 illustrates the variation of the thermal properties at elevated temperatures. The values given in Tables 2-4 and Fig. 19 can be used in the modelling of single and double plasterboard (thickness of 16 mm and density of 13 kg/m^2) sheathed walls if the failure times are less than or equal to 120 and 160 min, respectively. Further details of the material properties of gypsum plasterboard used in this study are given in Dodangoda et al. [7].

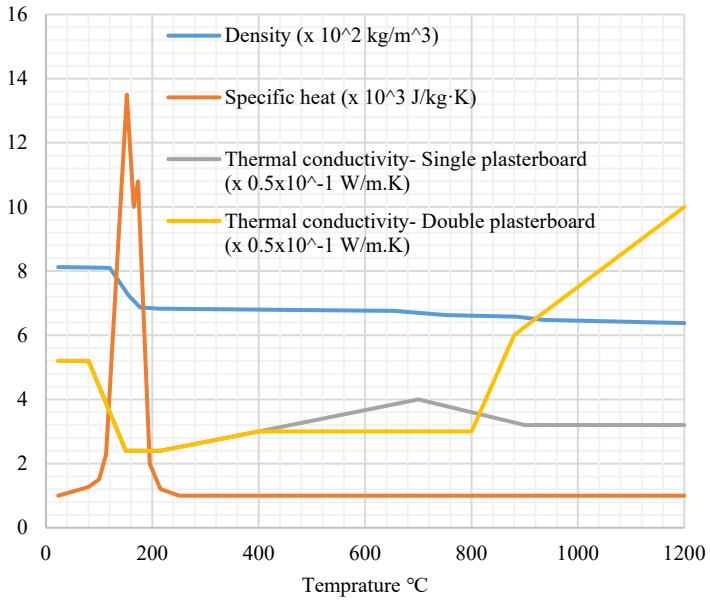

Fig. 19. Elevated temperature thermal properties of gypsum plasterboard.

3.2 Geometry and boundary conditions

Numerical models were developed using 8 node linear heat transfer brick elements (DC3D8) available in Abaqus software. Mesh sizes of 20 mm and 4 mm were assigned along the surface and the thickness of the plasterboard, respectively, similar to Ariyanayagam and Mahendran [17]. Heat transfer through solid surfaces in contact was simulated using tie constraints. As illustrated in Fig. 20, the convective heat transfer coefficients of 25 W/m^2°C and 10 W/m^2°C were assigned to the fire exposed and ambient sides of the plasterboard, respectively [1, 13, 17]. The emissivity of a surface is defined as its interaction with thermal radiation, in terms of emission and absorption. A high emissivity value indicates a high absorptance of radiation energy. Upon contact with flames, the paper layer of the fire side plasterboard burns and turns dark within 3 min, but the shiny paper layer on the unexposed surfaces (cavity and ambient sides) can survive for a considerable period of time. Hence, the emissivity value of the exposed side should be higher than that on the unexposed sides. Therefore, in contrast to the use of a constant emissivity value of 0.9 by many researchers [1, 5, 7, 17, 36], in this study emissivity values of 0.8 and 1.0 were assigned to the unexposed and exposed plasterboard surfaces, respectively, as suggested in Eurocode 1 Part 1-2 [37]. The heat transfer due to steam and hot gases inside the cavity was not simulated in this model. ISO 834 [23] standard fire curve and sink temperature of 20 ℃ were assigned to the fire and ambient side plasterboard surfaces, respectively, as surface film condition and surface radiation interaction.

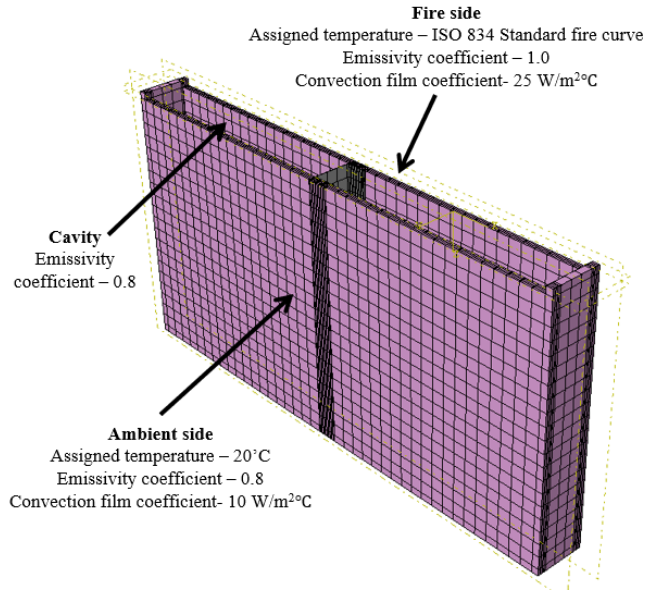

Fig. 20. Boundary conditions assigned in the heat transfer numerical model

Initially, two models of 2.4 m x 3.0 m and 0.6 m x 0.6 m were developed to investigate the effect of multiple studs and cavity size (Fig. 21). As shown in Fig. 22, the obtained plasterboard surface temperatures were similar for both scenarios indicating that the effect of cavity size perpendicular to the main direction of heat transfer is negligible. Therefore, a model size of 0.6 m x 0.6 m was used for further analyses similar to Ariyanayagam and Mahendran [17].

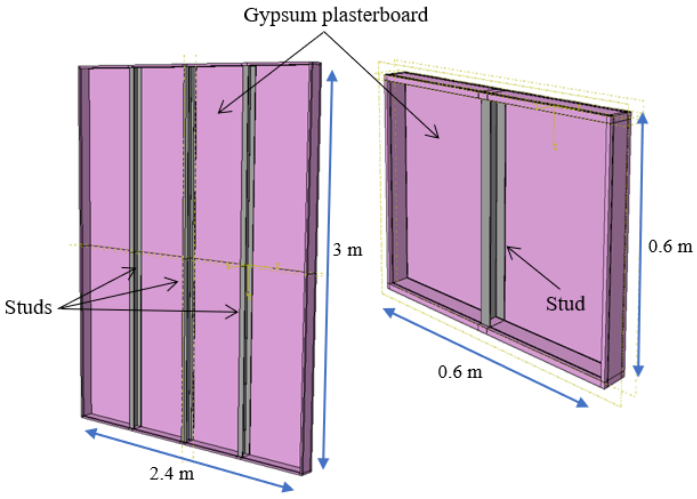

Fig. 21. Geometry of heat transfer models.

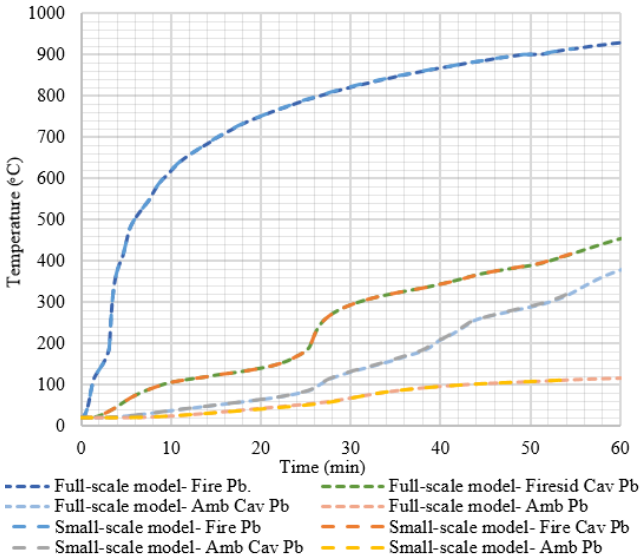

Fig. 22. Comparison of time-temperature profiles from 2.4 m x 3 m and 0.6 m x 0.6 m models.

Figs. 23 and 24 compare the time-temperature profiles of single and double plasterboard sheathed walls obtained from the developed heat transfer models and fire tests conducted in this study and by other researchers (Table 1). A reasonably good agreement can be seen between the numerical results and the average experimental results. Therefore, the developed heat transfer FE model assigned with the modified thermal properties can be used to accurately predict the time-temperature profiles of plasterboard surfaces of single and double plasterboard sheathed walls and stud temperatures of double plasterboard sheathed walls.

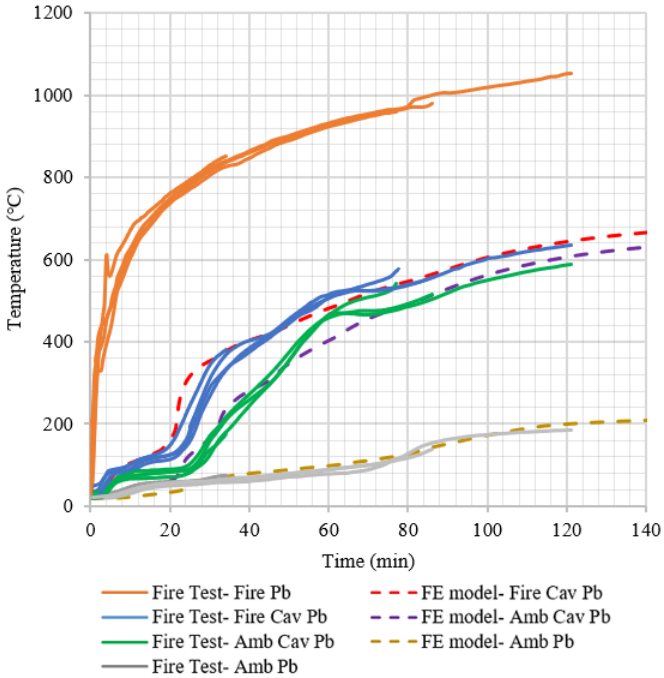

Fig. 23. Comparison of numerical and experimental time-temperature profiles of single plasterboard sheathed walls.

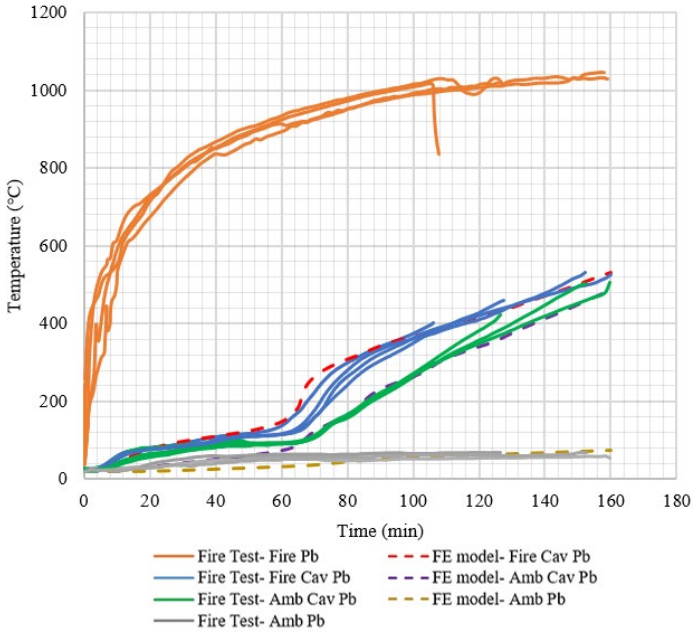

Fig. 24. Comparison of numerical and experimental time-temperature profiles of double plasterboard sheathed walls.

3.3 Modelling plasterboard fall-off

As discussed in Section 2.5, for single plasterboard sheathed walls, accurate stud temperature profiles cannot be determined from heat transfer models without integrating the effects of plasterboard joint opening. Hence the observed joint opening-up behaviour needs to be converted using geometric dimensions to numerically simulate it. It was clear that the plasterboard joint compound detached and fell off after about 17 min. Afterwards, it was assumed that the rest of the plasterboard joint compound trapped in the plasterboard joint was gradually detached. Then, a gradual increase in the gap between plasterboards was observed until failure. After the fire test, the average gap in the plasterboard joints was measured and it was about 4-5 mm at undisturbed locations. Considering all the above observations, the plasterboard joint fall-off and opening-up sequence were approximately categorised into six steps as shown in Table 5, and the corresponding element blocks are shown in Fig. 25.

The FE model was run for 17 min with undisturbed conditions and then the plasterboard joint filler (element block 1) was removed from it. Then the size of the plasterboard joint gap was gradually increased from 1 to 4 mm, by sequentially removing the element blocks 2, 3, 4, and 5 at 20, 25, 30 and 35 min, respectively. As soon as an element block is deleted, radiation and convective heat are assigned to the updated fire-exposed surface at the beginning of the following step. Fig. 26 illustrates the temperature contours at the end of each analysis step. The

temperature contours were parallel in the initial step and when the elements were deleted a sharp valley was formed in the plasterboard joint. Although this process is divided into six steps, the actual plasterboard fall-off happens smoothly.

Table 5. Sequence simulating plasterboard joint fall-off and opening-up.

Step	Function	Total time (min)
1	No element deletion	-
2	Delete element block 1	17
3	Delete element block 2	20
4	Delete element block 3	25
5	Delete element block 4	30
6	Delete element block 5	35

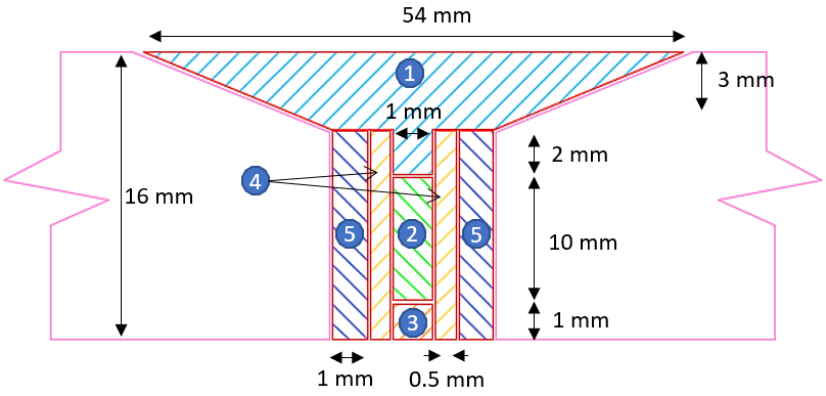

Fig. 25. Element blocks.

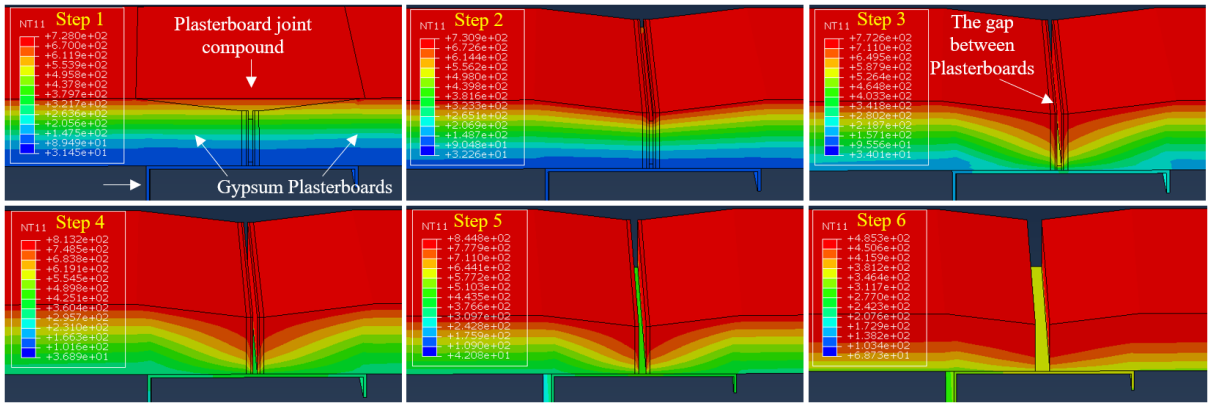

Fig. 26. Temperature contours after each step.

Fig. 27 compares the time-temperature profiles of hot flange of studs at the plasterboard joint from the heat transfer analyses and Fire Test T2. The heat transfer model including the plasterboard joint shows a good agreement with the fire test results, indicating that the chosen

number of steps is sufficient. A hot flange temperature difference of 140 ℃ was observed between numerical and fire test results when the plasterboard joint fall-off and opening-up was not simulated. This highlights the importance of incorporating the effects of plasterboard fall-off in the heat transfer FE models of single plasterboard sheathed LSF walls.

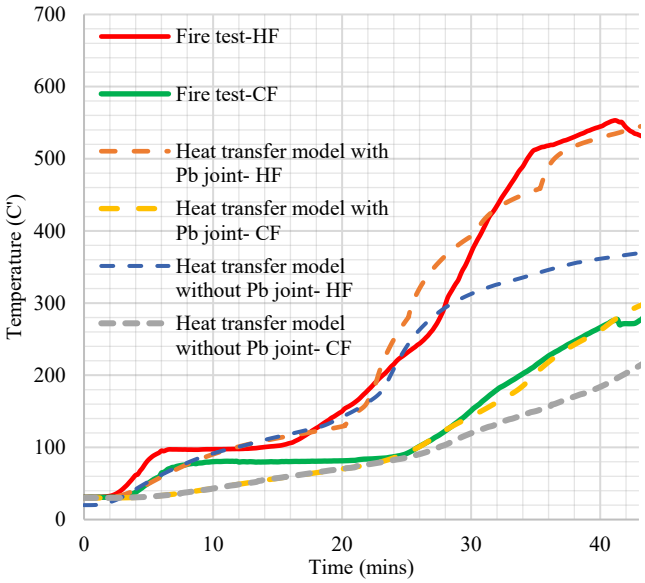

Fig. 27. Comparison of stud hot flange temperatures at the plasterboard joint from heat transfer analyses and Fire Test T2.

4 Structural behaviour of LSF walls exposed to fire

With increasing temperature, the strength and stiffness of LSF wall studs are gradually reduced. Hence the steel properties closer to the hot flange are subject to a higher reduction than for cold flange, due to the non-uniform temperature distribution. If the stud is subjected to uniform compression and no thermal bowing is present, there is a high chance for the hot flange to fail before the cold flange. Due to the non-uniform temperature distribution, the neutral axis of the stud shifts away from the fire side. Nevertheless, due to differential thermal expansion, thermal bowing of the stud occurs towards the furnace. The resultant shift of the neutral axis causes a bending moment in the stud which reduces and increases the compressive stresses in the hot and cold flanges at mid-height, respectively. If the stud is subject to high thermal bowing deflections, the failure could happen in the cold flange, followed by global buckling towards the furnace. However, the out-of-plane restraints provided by sheathing boards could potentially reduce the thermal bowing of the studs and influence their behaviour and failure. Hence a detailed investigation was conducted using experimental and numerical analyses to explore the effect of out-of-plane restraints provided by sheathing on the FRL of LSF walls.

4.1 Out-of-plane restraints provided by sheathing

The thermal bowing of stud is partially restrained by sheathing through the local in-plane (along stud length) and pull-through responses of screw connections, and the contact pressure between stud and sheathing, as illustrated in Fig. 28. The stresses in the stud are partially transferred to the sheathing boards through screw connections and contact pressure. The level of composite behaviour between stud and sheathing mainly depends on the local in-plane (along stud length) and pull-through behaviour of the stud-to-sheathing screw connections. Abeysiriwardena and Mahendran [38-39] proposed a method to simulate the local in-plane and pull-through behavioural characteristics using an iterative orthogonal non-linear spring pair model for ambient temperature. However, simulating temperature-dependent non-linear screw behaviour together with stud-to-sheathing contact interactions is complicated due to numerical convergence issues. Thus idealised out-of-plane linear springs are employed at screw locations to simulate the resultant out-of-plane restraints provided by sheathing and screw connections (Fig. 28). In this section, the effects of out-of-plane restraints provided by sheathing are investigated using the results from numerical models and fire tests of load-bearing LSF walls.

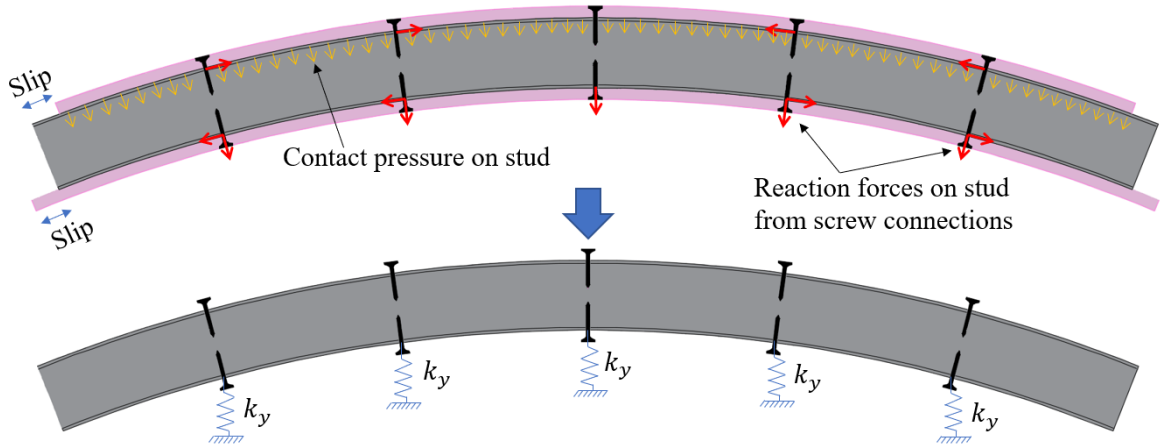

Fig. 28. Out-of-plane restraints provided by plasterboard sheathing.

The three fire tests conducted in this study (Fire Tests T1-T3) and another six fire tests conducted by Gunalan et al. [26] and Ariyanayagam and Mahendran [17, 28] (T4-T9) were selected for this investigation. Table 6 summarises the key details of Fire Tests T4-T9. The fire tests conducted in this study failed in distortional buckling associated with global buckling deformations, while the studs used in Fire Tests T4-T9 were prone to local buckling and hence failed predominantly by local buckling associated with global buckling deformations.

Table 6. Details of selected full-scale fire tests of load-bearing LSF walls.

Test No.	Research study	Stud dimensions (mm)	Wall height (m)	Plasterboard Layers	Cavity insulation
T4	Ariyanayagam and Mahendran [28]	92 x 35 x 8 x 1.15	3.0	2	none
T5	Gunalan et al. [26]	90 x 40 x 15 x 1.15	2.4	2	none
T6	Gunalan et al. [26]	90 x 40 x 15 x 1.15	2.4	2	glass fibre
T7	Ariyanayagam and Mahendran [17]	92 x 35 x 8 x 1.15	3.0	1	none
T8	Ariyanayagam and Mahendran [17]	92 x 35 x 8 x 1.15	3.0	1	glass fibre
T9	Gunalan et al. [26]	90 x 40 x 15 x 1.15	2.4	1	none

4.2 Development of structural FE model

Due to the high cost associated with full scale fire testing, validated numerical models are often employed to predict the structural failure times of LSF walls in fire. Once the time-temperature profiles of studs are obtained, transient or steady-state non-linear structural FE analysis is performed to predict their failure times. To simplify the numerical problem, many researchers [13-17] have modelled a single stud with simplified boundary conditions to simulate the interaction with tracks and plasterboard sheathing. Although, the in-plane restraint (perpendicular to the stud length) provided by sheathing is considered in the FE models, the effect of out-of-plane restraint is ignored.

Numerical models are solved using transient or steady-state coupled temp-displacement analysis. In the transient analysis, a pre-determined load is applied at the beginning and maintained while the assigned non-uniform temperature distribution is increased until the failure of the stud. In the steady-state analysis, the non-uniform temperature distribution is kept the same, and the load is gradually increased until failure. Ariyanayagam and Mahendran [40] showed that both analysis methods predict similar failure times. However, the transient analysis is similar to the way fire testing is conducted and additional valuable information like the lateral displacement variation with time can be obtained. Therefore, transient coupled temp-displacement analysis was performed in this study.

Fig. 29 illustrates the single stud model developed in Abaqus software. The stud was modelled using a 4 mm mesh of four-node quadrilateral shell elements with reduced integration and temperature degree of freedom (S4RT elements). Local buckling mode shape determined from elastic buckling analysis was assigned to non-linear analysis. The magnitude of geometric imperfections and the coefficient of thermal expansion were calculated as per AS/NZS 4600 [41]. The measured elastic modulus and yield stress at ambient temperature were used to derive the reduced elastic modulus and yield stress at elevated temperature as proposed in AS/NZS 4600 [41]. The stress-strain characteristics at elevated temperatures were calculated using the two-stage non-linear stress-strain model proposed by Rokilan and Mahendran [42]. Moreover, the effects of geometric nonlinearities were incorporated in the numerical analysis.

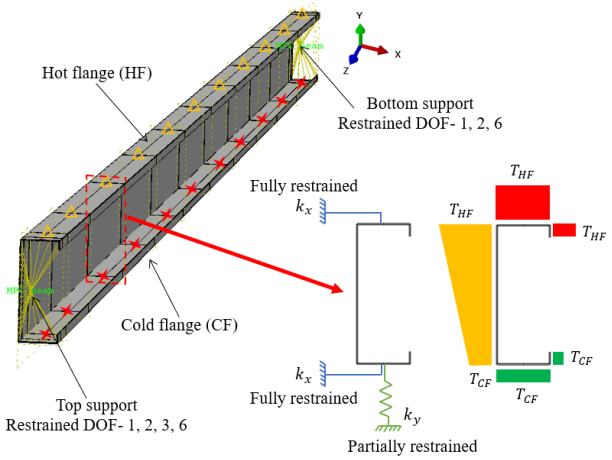

Fig. 29. Structural FE model.

The rotational degree of freedom about the z-axis and all translational degree of freedoms at the stud ends were restrained except for the z-translational degree at the bottom, where the load was applied similar to the fire tests. The x-degree of freedom at screw locations on both hot and cold flanges were fully restrained and linear out-of-plane springs were assigned at screw locations on the cold flange. The hot and cold flange temperatures of the failed studs measured in the fire tests were assigned to the respective flanges and their adjacent lips, and a linear temperature variation was assumed across the stud web, as shown in Fig. 29. The analysis was repeated by gradually increasing the stiffness of out-of-plane springs (k_y) to understand the effects of plasterboard sheathing.

4.3 Failure modes and overall behaviour

The stiffness of out-of-plane springs was gradually increased from 0 to 8 N/mm at 1 N/mm interval and the lateral displacement (at the midpoint of the stud's cold flange at mid-height) versus time curve was plotted and the stud failure time determined in each case. Fig. 30 shows the lateral displacement versus time plots obtained from FE analysis for Fire Test T4 (Table 6). As the out-of-plane restraint was increased, a gradual reduction in lateral displacement was observed. With little or no out-of-plane restraint, high thermal bowing was observed and the dominant failure mode was global buckling towards the furnace induced by the local buckling of cold flange, as shown in Fig. 31. When the out-of-plane restraint was increased from 0 to 3 N/mm, the FRL (failure time) increased by 23%. Once the out-of-plane restraint was increased beyond 3 N/mm, the lateral deflection was further reduced, increasing the compressive stresses on the hot flange and therefore, the failure location changed from cold flange to hot flange, as shown in Fig. 31. Once the failure location is changed to hot-flange, further increase in out-of-plane restraint resulted in a reduction of failure times. Hot or cold flange failures resulted in lateral movement of the wall away from or towards the furnace, respectively. Thus, the location of stud failure can be identified using the direction of lateral movement of the stud at failure. It is important to note that, providing excessive out-of-plane restraints, such as lining the studs with steel sheathing, could possibly adversely affect the FRLs of LSF walls.

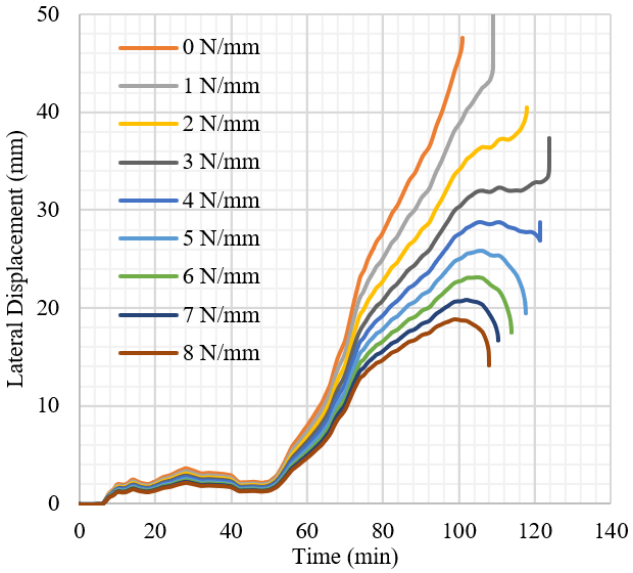

Fig. 30. Lateral displacement versus time plots for Test T4.

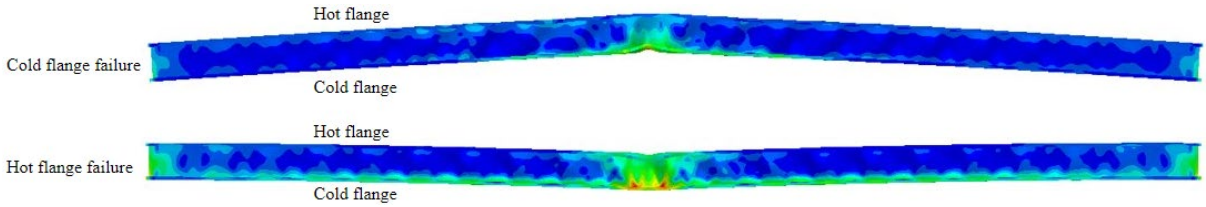

Fig. 31. Failure modes.

4.4 Determining the idealised out-of-plane restraint values

Both experimental and numerical results were used and compared to determine the idealised out-of-plane restraint values provided by gypsum plasterboard sheathing. In the fire tests, the lateral displacements are measured by LVDTs located on the ambient side of the plasterboard (Fig. 5) and in FE models the displacements of studs are directly extracted. Thus experimental and numerical lateral displacements cannot be directly compared to validate the numerical models. However, the overall direction of the lateral movement and failure times can be used to determine the equivalent out-of-plane restraints provided by gypsum plasterboards.

Fig. 32 illustrates the variation of lateral displacement versus time plots with out-of-plane restraints for double plasterboard sheathed LSF wall configurations used in Fire Tests T3 to T6 (Table 6). The failure times obtained from Fire Test T3 (this study) and FE analysis agreed well when the out-of-plane restraint value was 3 N/mm. However, the experimental lateral displacement plot of Fire Test T3 (Fig. 32 (e)) shows that the tested wall moved away from the furnace at failure. This phenomenon was predicted by the numerical model when the out-of-plane restraints was increased to 5 N/mm (Fig. 32 (a)). In Fire Test T4, the failure time and failure mode from FE analysis agreed well with experimental results when the out-of-plane restraint was 3 N/mm. A significant failure time variation was observed when the out-of-plane restraint was varied for 3 m long studs (Figs. 32 (a) and (b)), but it was minimal for 2.4 m long studs (Figs. 32 (c) and (d)), ie. the effect of out-of-plane restraints on the FRL is significant for slender studs. This could be the reason why the researchers who conducted the fire tests of 2.4 m high walls [14-15] disregarded the effects of out-of-plane restraints in their numerical analyses. Therefore, determining the equivalent out-of-plane restraint for 2.4 m wall tests (T5 and T6) using the failure times is not viable as its variation is minimal. However, in Test T6, the failure location can be identified as the hot flange based on the stud's lateral movement away from the furnace (Fig. 32 (e)). The numerical model showed that the hot flange failure occurred in this case when the out-of-plane restraint was increased above 3 N/mm. Therefore, the equivalent out-of-plane restraint value for Test T6 should be more than or equal to 3 N/mm.

A study conducted by Dias [22] also showed that using two gypsum plasterboards provide an out-of-plane restraint of 2.85 N/mm. Therefore, it can be concluded that the out-of-plane restraints provided by two 16 mm plasterboards is equivalent to spring stiffness of around 3 to 5 N/mm when the failure times are in the range of 100 to 120 min. This value could decrease or increase when the failure time is more than 120 min or less than 100 min, respectively, because of changing material properties of gypsum plasterboards with fire exposure time.

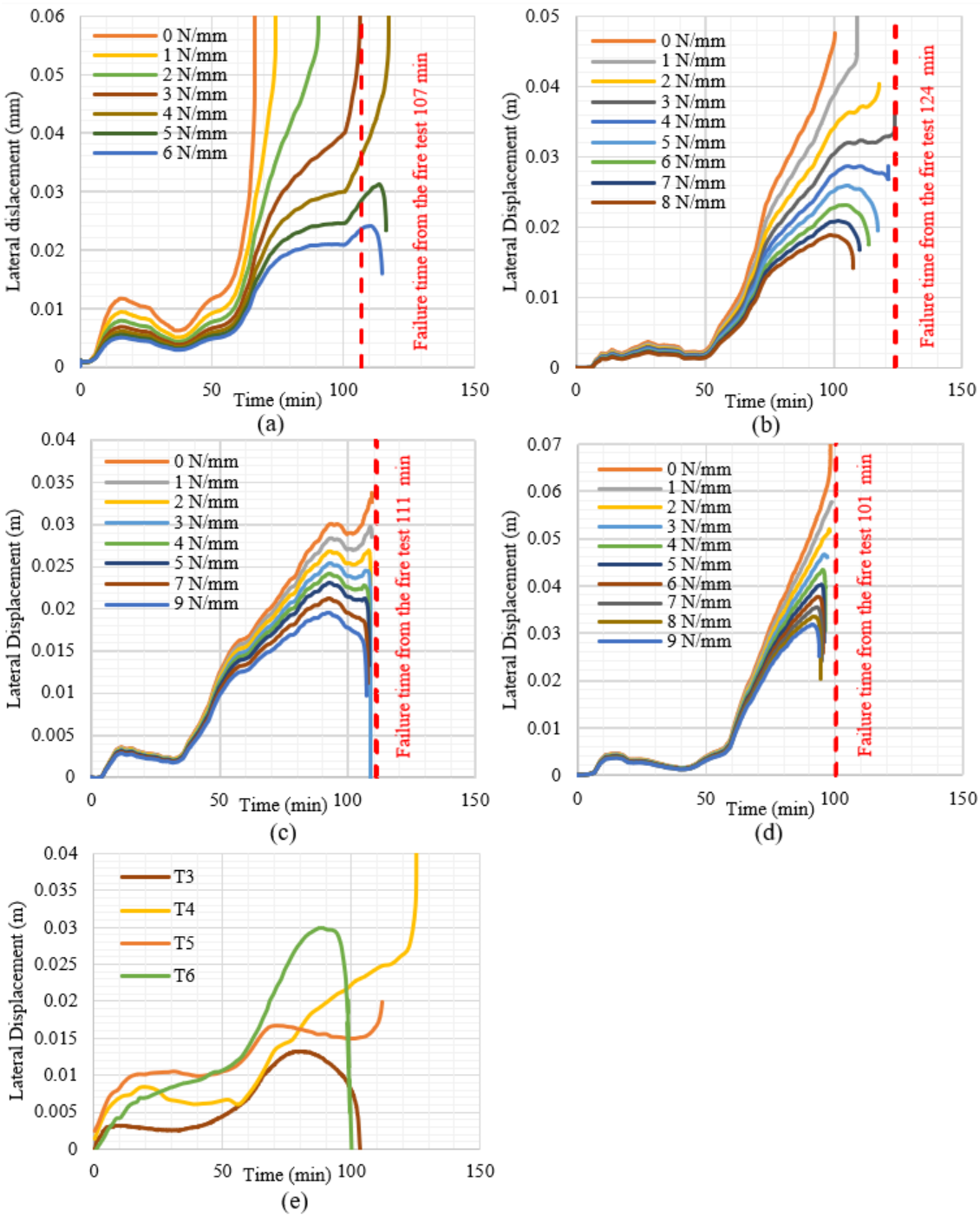

Fig. 32. Lateral displacement versus time plots from numerical trials for fire tests of double plasterboard sheathed walls a) T3, b) T4, c) T5, d) T6 and e) their experimental results.

Similar to the observations of double plasterboard sheathed LSF walls, large variations in failure times were observed for 3 m long studs as shown in Figs. 33 (a)-(d), and no distinctive difference in failure time or mode was observed for 2.4 m long studs in Fire Test T9 (Fig. 33 (e)) for single plasterboard sheathed LSF walls. Therefore, Fire Test T9 results could not be used to determine the idealised out-of-plane restraint values. In Fire Tests T1 (Fig. 33 (a)) and T8 (Fig. 33 (d)), the experimental failure time and failure locations agreed well with the FE results obtained with the out-of-plane restraints in the ranges of 2 - 3 N/mm and 1 – 2 N/mm, respectively. In Fire Test T2, experimental and numerical failure times agreed well when the out-of-plane restraint was 3 N/mm, however, the correct failure mode was obtained with about 6 N/mm (Fig. 33 (b)). This increased out-of-plane restraint value could be due to the lower fire exposure time of Test T2 compared to other single plasterboard sheathed fire tests. Nevertheless, for Test T7, experimental failure times agreed well with the numerical model with no out-of-plane restraints. The deterioration of screw connection performance with increasing temperature [20] is the main reason for this as Test T7 was exposed to an additional 33 min of ISO 834 standard fire. Therefore, it can be concluded that the out-of-plane restraints provided by single plasterboard sheathing vary from 3 to 1 N/mm after 35 to 50 min of ISO 834 standard fire exposure, and reduce to zero after 80 min exposure. Additionally, the out-of-plane restraint values are expected to be higher than 3 N/mm for lower exposure times.

In summary, the gypsum plasterboard sheathing is capable of providing out-of-plane restraints to the LSF wall studs, in addition to in-plane restraints. These out-of-plane restraints reduce the thermal bowing deflections and as a result, the bending moment induced by the eccentricity is reduced. The difference in failure times obtained from numerical analysis with and without out-of-plane restraints was as high as 40% in some cases, which highlights the importance of incorporating the effects of out-of-plane restraints in the structural FE modelling of LSF walls exposed to fire conditions. Furthermore, it was observed that the out-of-plane restraints provided by sheathing boards depend on the fire exposure time, since the material properties of gypsum plasterboards and the performance of stud-to-sheathing screw connections gradually deteriorate [20] with increasing fire exposure time, resulting in reduced out-of-plane restraint values. Table 7 presents the proposed out-of-plane restraint values as a function of fire exposure time.

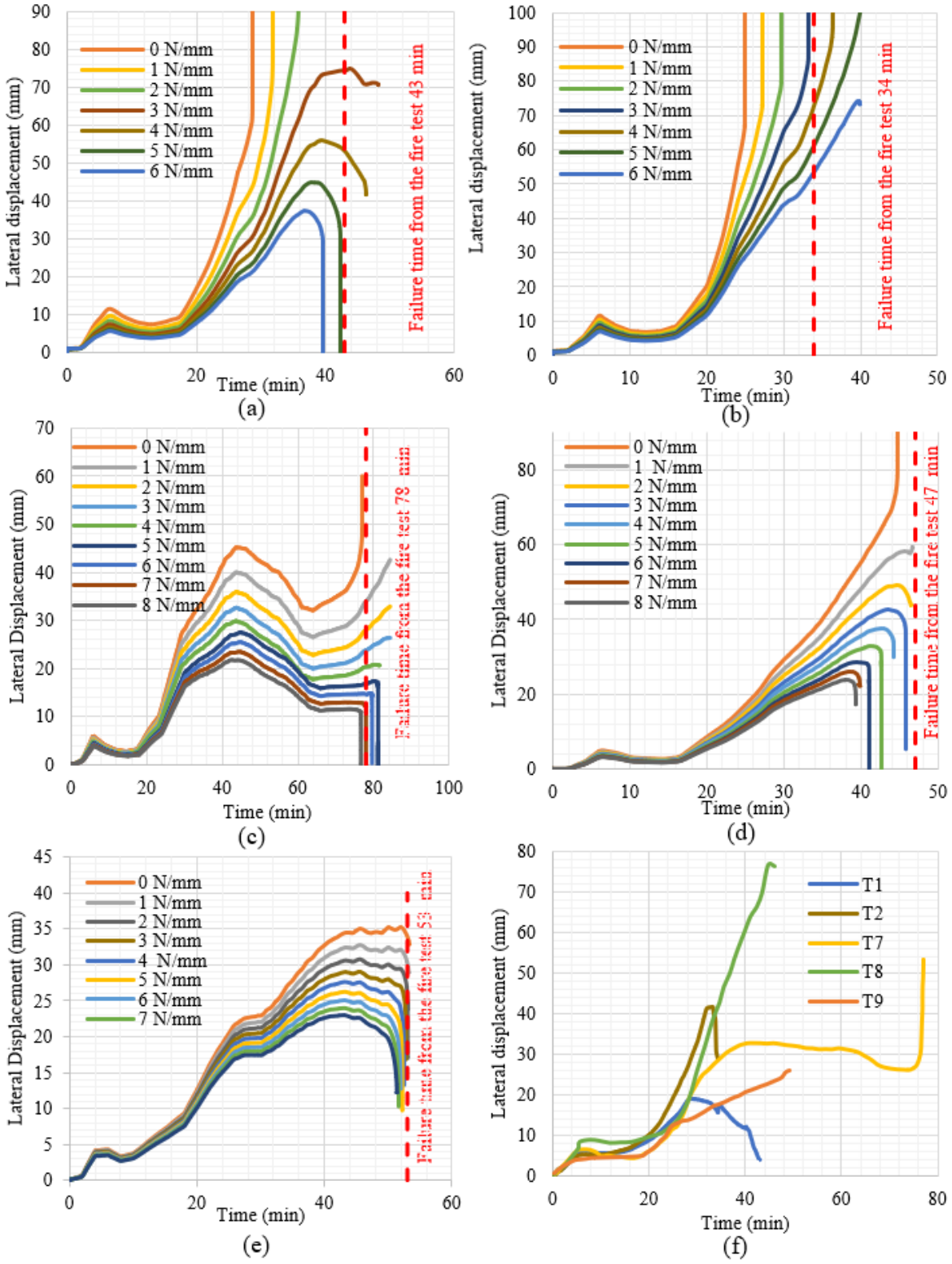

Fig. 33. Lateral displacement versus time plots from numerical trials for fire tests of single plasterboard sheathed walls a) T1, b) T2, c) T7, d) T8, e) T9 and f) their experimental results.

Table 7. Out-of-plane restraints provided by gypsum plasterboard sheathing

Wall configuration	Time (min)	k_y (N/mm)
Double plasterboard sheathed	100-120	3-5
Single plasterboard sheathed	35-45	2-3
	45-50	1-2
	≥80	0

5 Conclusions

This paper has presented the details of a study based on numerical modelling and fire tests to enhance the understanding of the thermal and structural behaviour of LSF walls and to facilitate accurate thermal and structural modelling of LSF walls exposed to fire conditions. It has addressed two main research gaps related to the behaviour of LSF walls in fire, the first being their heat transfer behaviour, especially at plasterboard joints, and the second being their structural behaviour, and the effects of out-of-plane restraints provided by gypsum plasterboard sheathing. For this purpose, three full-scale standard fire tests of LSF walls were conducted first, and their results together with those from previously conducted fire tests were used with heat transfer and structural FE modelling of LSF walls.

The heat transfer behaviour of single and double plasterboard sheathed LSF walls was investigated using the fire test results, which led to the identification of key parameters and the development of idealised time-temperature envelopes for use in parametric numerical studies. Fire test observations using a furnace camera showed that the most vulnerable location for LSF wall stud was the plasterboard joint and that most of the plasterboard joint compound fell off after about 17 min of standard fire exposure, following which the plasterboard joint gap gradually increased allowing further heat penetration directly to the stud hot flanges. Using the heat transfer FE model and the time-temperature profiles of fire tests, improved apparent thermal conductivity material properties of gypsum plasterboards were proposed for use in heat transfer models. This study has shown that conventional heat transfer models are adequate to simulate the thermal behaviour of double plasterboard sheathed LSF walls exposed to fire, however, due to plasterboard joint opening-up and plasterboard fall-off, they predicted lower stud temperatures for single plasterboard sheathed walls. Therefore, a multi-step heat transfer model was developed, incorporating the physical changes in the fire side plasterboard joint, to accurately simulate the plasterboard joint effects on the behaviour of LSF walls in fire. It is

recommended that the visual observations of fire side sheathing boards are incorporated in future numerical studies, instead of simply increasing thermal conductivity to simulate the effects of plasterboard fall-off and plasterboard joint opening-up.

Investigating the structural behaviour of LSF walls in fire using FE models is preferred due to the high cost and time associated with full-scale fire tests. However, the effects of out-of-plane restraints provided by gypsum plasterboard sheathing were not considered by many past research studies. This study has investigated the effect of out-of-plane restraints provided by plasterboard sheathing using a single stud FE model with simplified boundary conditions and the results of fire tests conducted in this study and those available in the literature. The results showed that FRL of LSF walls is significantly improved by the out-of-plane restraints of 16 mm thick gypsum plasterboard sheathing. By comparing experimental and numerical failure times and failure modes, suitable out-of-plane restraints values have been recommended for use in structural FE analyses of single and double plasterboard sheathed walls.

Acknowledgements

The authors wish to thank Australian Research Council (Grant Number LP170100951) and National Association of Steel Framed Housing (NASH) for providing financial support and QUT for providing the required research facilities. They appreciate the valuable technical guidance and support provided by NASH Executive Director Ken Watson, and NASH Standards Committee members to this research study. They also extend their appreciation to the technical staff at Banyo Laboratory (QUT) for their support to the experimental study. Finally, the authors acknowledge the generous contributions of Bluescope Steel, Enduroframe and USG Boral in providing the required CFS studs and plasterboards.

References

1. Rusthi, M., Keerthan, P., Mahendran, M., & Ariyanayagam, A. (2017). Investigating the fire performance of LSF wall systems using finite element analyses. Journal of Structural Fire Engineering, 8(4), 354-376.
2. Mehaffey, J. R., Cuerrier, P., & Carisse, G. (1994). A model for predicting heat transfer through gypsum-board/wood-stud walls exposed to fire. Fire and materials, 18(5), 297-305.
3. Thomas, G. (2002). Thermal properties of gypsum plasterboard at high temperatures. Fire and materials, 26(1), 37-45.
4. Wakili, K. G., & Hugi, E. (2009). Four types of gypsum plaster boards and their thermophysical properties under fire condition. Journal of Fire Sciences, 27(1), 27-43.
5. Keerthan, P., & Mahendran, M. (2012). Numerical studies of gypsum plasterboard panels under standard fire conditions. Fire Safety Journal, 53, 105-119.
6. Yu, Q. L., & Brouwers, H. J. H. (2012). Thermal properties and microstructure of gypsum board and its dehydration products: a theoretical and experimental investigation. Fire and Materials, 36(7), 575-589.
7. Dodangoda, M. T., Mahendran, M., Pologanathan, K., & Frost, R. (2016). Material characterisation and numerical modelling of gypsum plasterboards in fire. In Structures in fire: Proceedings of the 9th International Conference (pp. 1116-1123). DEStech Publications.
8. Sultan, M. A. (2008). Fall-off of gypsum plasterboard in fire. In The Fifth International Conference on Structures in Fire (SiF08), (pp. 644-655).
9. Ariyanayagam, A. D., Kesawan, S., & Mahendran, M. (2016). Detrimental effects of plasterboard joints on the fire resistance of light gauge steel frame walls. Thin-Walled Structures, 107, 597-611.
10. Gnanachelvam, S., Ariyanayagam, A., & Mahendran, M. (2019). Fire resistance of light gauge steel framed wall systems lined with PCM-plasterboards. Fire Safety Journal, 108, 102838.
11. Steau, E., & Mahendran, M. (2020). Fire resistance behaviour of LSF floor-ceiling configurations. Thin-Walled Structures, 156, 106860.
12. Tao, Y., Mahendran, M., & Ariyanayagam, A. (2021). Numerical study of LSF walls made of cold-formed steel hollow section studs in fire. Thin-Walled Structures, 167, 108181.

13. Feng, M., Wang, Y. C., & Davies, J. M. (2003). Axial strength of cold-formed thin-walled steel channels under non-uniform temperatures in fire. Fire Safety Journal, 38(8), 679-707.
14. Gunalan, S., & Mahendran, M. (2013). Finite element modelling of load bearing cold-formed steel wall systems under fire conditions. Engineering Structures, 56, 1007-1027.
15. Kesawan, S., & Mahendran, M. (2016). Predicting the performance of LSF walls made of hollow flange channel sections in fire. Thin-Walled Structures, 98, 111-126.
16. Rusthi, M., Ariyanayagam, A. D., & Mahendran, M. (2018). Fire design of LSF wall systems made of web-stiffened lipped channel studs. Thin-Walled Structures, 127, 588-603.
17. Ariyanayagam, A. D., & Mahendran, M. (2019). Influence of cavity insulation on the fire resistance of light gauge steel framed walls. Construction and Building Materials, 203, 687-710.
18. Rokilan, M., & Mahendran, M. (2022). Design of cold-formed steel wall studs subject to non-uniform elevated temperature distributions. Thin-Walled Structures, 171, 108625.
19. Kesti, J. (2000). Local and distortional buckling of perforated steel wall studs, Doctoral dissertation, Helsinki University of Technology, Espoo, Finland.
20. Abeysiriwardena, T., Peiris, M., & Mahendran, M. (2021a). Behaviour of stud-to-sheathing fastener connections in LSF walls at elevated temperatures. Engineering Structures, 238, 112224.
21. Vieira Jr, L. C. M., & Schafer, B. W. (2013). Behavior and design of sheathed cold-formed steel stud walls under compression. Journal of Structural Engineering, 139(5), 772-786.
22. Dias, H. Y. V. (2019). Structural and fire behaviour of gypsum plasterboard and steel sheathed LSF walls (Doctoral dissertation, Queensland University of Technology).
23. ISO 834-1, (1999), Fire Resistance Tests-Elements of Building Construction, Part1: General Requirements, International Organization for Standardization, Geneva, Switzerland.
24. Alfawakhiri, F., Sultan, M. A., & MacKinnon, D. H. (1999). Fire resistance of loadbearing steel-stud wall protected with gypsum board: a review. Fire technology, 35(4), 308-335.

25. Feng, M., & Wang, Y. C. (2005). An experimental study of loaded full-scale cold-formed thin-walled steel structural panels under fire conditions. Fire Safety Journal, 40(1), 43-63.
26. Gunalan, S., Kolarkar, P., & Mahendran, M. (2013). Experimental study of load bearing cold-formed steel wall systems under fire conditions. Thin-Walled Structures, 65, 72-92.
27. Kesawan, S., & Mahendran, M. (2015). Fire tests of load-bearing LSF walls made of hollow flange channel sections. Journal of Constructional Steel Research, 115, 191-205.
28. Ariyanayagam, A. D., & Mahendran, M. (2018). Fire performance of load bearing LSF wall systems made of low strength steel studs. Thin-Walled Structures, 130, 487-504.
29. Feng, M., Wang, Y. C., & Davies, J. M. (2018). Behaviour of Loaded Full-Scale Cold-Formed Thin-Walled Steel Structural Panels Under Fire Conditions. In Thin-Walled Structures (pp. 307-314). CRC Press.
30. Dias, Y., Mahendran, M., & Poologanathan, K. (2019). Axial compression strength of gypsum plasterboard and steel sheathed web-stiffened stud walls. Thin-Walled Structures, 134, 203-219.
31. Magarabooshanam, H., Ariyanayagam, A., & Mahendran, M. (2019). Behaviour of load bearing double stud LSF walls in fire. Fire Safety Journal, 107, 15-28.
32. Tao, Y., Mahendran, M., & Ariyanayagam, A. (2021). Fire tests of cold-formed steel walls made of hollow section studs. Journal of Constructional Steel Research, 178, 106495.
33. EN 1993-1-2: 2005, Eurocode 3: Design of steel structures. Part 1-2: General Rules - Structural Fire Design, European Committee for Standardization, Brussels, 2005.
34. ASTM E1269-11: 2005, ASTM International: Standard test method for determining specific heat capacity by differential scanning calorimetry, 2005.
35. Frangi, A., Schleifer, V., Fontana, M., & Hugi, E. (2010). Experimental and numerical analysis of gypsum plasterboards in fire. Fire technology, 46(1), 149-167.
36. Wakili, K., Hugi, E., Wullschleger, L., & Frank, T. H. (2007). Gypsum board in fire—modeling and experimental validation. Journal of fire Sciences, 25(3), 267-282.
37. EN 1991-1-2 2002, Eurocode 1: Actions on structures - Part 1-2: General actions - Actions on structures exposed to fire, CEN, Bruxelles, 2005.

38. Abeysiriwardena, T., & Mahendran, M. (2022). Experimental and numerical investigations of LSF walls subject to distortional buckling. Thin-Walled Structures, 171, 108685.
39. Abeysiriwardena, T., Peiris, M., & Mahendran, M. (2021b). Local in-plane strength and stiffness of stud-to-sheathing fastener connections in LSF wall panels. Thin-Walled Structures, 160, 107383.
40. Ariyanayagam, A. D., & Mahendran, M. (2014). Numerical modelling of load bearing light gauge steel frame wall systems exposed to realistic design fires. Thin-Walled Structures, 78, 148-170.
41. Standards Australia. (2018). Cold-formed Steel Structures (AS/NZS 4600), Sydney, Australia.
42. Rokilan, M., & Mahendran, M. (2020). Elevated temperature mechanical properties of cold-rolled steel sheets and cold-formed steel sections. Journal of Constructional Steel Research, 167, 105851.